

Transition densities and sample frequency spectra of diffusion processes with selection and variable population size

Daniel Živković^{a,*}, Matthias Steinrücken^b, Yun S. Song^{b,c}, Wolfgang Stephan^a

^a*Section of Evolutionary Biology, Department of Biology, Ludwig-Maximilian University Munich, Munich, Germany*

^b*Department of Statistics, University of California, Berkeley, California 94720, USA*

^c*Computer Science Division, University of California, Berkeley, California 94720, USA*

Abstract

Advances in empirical population genetics have made apparent the need for models that simultaneously account for selection and demography. To address this need, we here study the Wright-Fisher diffusion under selection and variable effective population size. In the case of genic selection and piecewise-constant effective population sizes, we obtain the transition density function by extending a recently developed method for computing an accurate spectral representation for a constant population size. Utilizing this extension, we show how to compute the sample frequency spectrum (SFS) in the presence of genic selection and an arbitrary number of instantaneous changes in the effective population size. We also develop an alternate, efficient algorithm for computing the SFS using a method of moments. We apply these methods to answer the following questions: If neutrality is incorrectly assumed when there is selection, what effects does it have on demographic parameter estimation? Can the impact of negative selection be observed in populations that undergo strong exponential growth?

*Corresponding author.

Email address: zivkovic@bio.lmu.de (Daniel Živković)

Introduction

1

2 Advances in empirical population genetics have pointed out the need for models that simultane-
3 ously account for selection and demography. Studies on samples from various species including
4 humans (e.g., Williamson et al. 2005; Tennessen et al. 2012) and *Drosophila melanogaster* (Glinka
5 et al. 2003; Duchon et al. 2013) have shown that demographic processes such as population size
6 changes shape in large part the patterns of polymorphism among genomes and estimated the im-
7 pact of selection on top of such underlying neutral conditions. Thus far, most theoretical papers
8 considered selective and demographic forces independently of each other for the sake of simplicity
9 (e.g., Stephan and Li 2007).

10 Theoretical studies of neutral models of time-varying population size have been accomplished
11 within the diffusion and the coalescent frameworks. Kimura (1955a) derived the transition density
12 function of the Wright-Fisher (WF) diffusion with a constant population size that characterizes the
13 neutral evolution of allele frequencies over time. Shortly thereafter, Kimura (1955b) noted how
14 to rescale time to generalize this result to a deterministically changing population size. Nei et al.
15 (1975) derived the average heterozygosity under this general condition by applying a differential
16 equation method, before studies on time-varying population size started to utilize the coalescent.
17 Watterson (1984) derived the probability distribution and the moments of the total number of alle-
18 les in a sample using models of one or two sudden changes in population size. Slatkin and Hudson
19 (1991) considered the distribution of pairwise differences in exponentially growing populations,
20 before Griffiths and Tavaré (1994) provided the coalescent for arbitrary deterministic changes in
21 population size. The allele frequency spectrum, which is the distribution of the number of times
22 a mutant allele is observed in a sample of DNA sequences, has been utilized in many theoretical
23 and empirical studies. It can be further distinguished into the allelic spectrum and the sample fre-
24 quency spectrum (SFS) according to whether absolute or relative frequencies are meant. Fu (1995)
25 derived the first- and second-order moments of the allelic spectrum for a constant population size,
26 which has been generalized to time-varying population size by Griffiths and Tavaré (1998) and
27 Živković and Wiehe (2008). Although deterministic fluctuations in population size are commonly
28 considered for the interpretation of biological data, studies have also examined stochastic changes
29 in population size (e.g., Kaj and Krone 2003).

30 The mathematical modeling of natural selection was mostly carried out within the diffusion
31 framework, whereas coalescent approaches have proven analytically tedious (e.g., Krone and

32 Neuhauser 1997). Fisher (1930) derived the equilibrium solution for the allelic spectrum of
33 a population, which became particularly useful when Sawyer and Hartl (1992) modeled the
34 frequencies of mutant sites via a Poisson random field approach. Kimura (1955c) employed a
35 perturbation approach to obtain a series representation of the transition density function that is
36 accurate for scaled selection coefficients smaller than one. However, as noted in Williamson et al.
37 (2005), an appropriate use of this result with respect to the analysis of whole-genome data is even
38 difficult for a constant population size. In a recent paper, Song and Steinrücken (2012) devised
39 an efficient method to accurately compute the transition density functions of the WF diffusion
40 with recurrent mutations and general diploid selection. This nonperturbative approach that can
41 be applied to scaled selection coefficients substantially greater than one finds the eigenvalues and
42 the eigenfunctions of the diffusion generator and leads to an explicit spectral representation of the
43 transition density function. The results for this biallelic case have been extended to an arbitrary
44 number of alleles by Steinrücken et al. (2013).

45 In recent years, several researchers have started to investigate the combined effect of natural
46 selection and demography. The majority of these studies have utilized finite difference schemes to
47 make results applicable. Williamson et al. (2005) employed such a scheme to obtain a numerical
48 solution for the SFS for a model with genic selection and one instantaneous population size change.
49 The authors applied this result within a likelihood-based method to infer population growth and
50 purifying selection at non-synonymous sites across the human genome. Evans et al. (2007) investi-
51 gated the forward diffusion equation with genic selection and deterministically varying population
52 size and incorporated the effect of point mutations via a suitable boundary condition. They derived
53 a system of ODEs for the moments of the allelic spectrum, but had to resort to a numerical scheme
54 to make their results applicable. Gutenkunst et al. (2009) considered population substructure and
55 selection to obtain the joint allele frequency spectrum of up to three populations by approximat-
56 ing the associated diffusion equation by a finite difference scheme as well. Lukić and Hey (2012)
57 applied spectral methods that even account for a fourth population in the otherwise same setting
58 as Gutenkunst et al. (2009). Recently, and again with respect to a single population, Zhao et al.
59 (2013) provided a numerical method to solve the diffusion equation for random genetic drift that
60 can incorporate the forces of mutation and selection. The authors illustrated the accuracy of their
61 discretization approach by determining the probability of fixation in the presence of selection for
62 both an instantaneous population size change and a linear increase in population size. In general,
63 such methods require an appropriate discretization of grid points, which may depend strongly on

64 the parameters. This makes it difficult, however, to predict if a particular discretization will produce
65 accurate results.

66 In this study, we use the polynomial approach by Song and Steinrücken (2012) to obtain the
67 transition density function for genic selection and instantaneous changes in population size. First,
68 we focus on a single time period during which the population has a different size relative to a fixed
69 reference population size. We compute the eigenvalues and the eigenfunctions of the diffusion
70 operator with respect to the modified drift term of the underlying diffusion equation. Similarly to
71 a constant population size, the eigenfunctions are given as a series of orthogonal functions. The
72 eigenvalues and eigenfunctions facilitate a spectral representation of the transition density function
73 describing the change in allele frequencies across this time period. Such transition densities for
74 single time periods can then be folded over various instantaneous population size changes to obtain
75 the overall transition density function for such a multi-epoch model with genic selection. After
76 illustrating the applicability of this approach, we derive the SFS by means of the transition density
77 function. While the transition density function proves useful for the analysis of time-series data that
78 are mostly gathered from species with short generation times as bacteria (e.g., Lenski 2011) but
79 also from species with long generation times (Steinrücken et al. 2014), the SFS can also be applied
80 to whole-genome data collected at a single time point. As an alternative approach to employing the
81 transition density function for the SFS, we modify the method of moments by Evans et al. (2007)
82 to efficiently compute allele frequency spectra for genic selection, point mutations and piecewise
83 changes in population size.

84 We then employ a maximum likelihood method to estimate the demographic and selective pa-
85 rameters of a given bottleneck model. After examining the accuracy of parameter estimation, we
86 discuss how the estimates change when selection is ignored or a simpler demographic model is
87 assumed. In this context, we investigate the demography of an African population of *Drosophila*
88 *melanogaster* (Duchen et al. 2013) by assuming both a selective and a neutral model. Furthermore,
89 we answer an other, important question arising in human population genetics (Tennessen et al.
90 2012): Can the impact of negative selection be observed in populations that undergo strong expo-
91 nential growth? We investigate, how strong selection would have to be to leave a signature in the
92 SFS.

93 The transition density function for genic selection and piecewise-constant
 94 population sizes with K epochs

95 **Model and notation**

96 We assume that the diploid effective population size changes deterministically, with $N(t)$ denoting
 97 the size at time t . Here, time is measured in units of $2N_{\text{ref}}$ generations, where N_{ref} is a fixed
 98 reference population size. Unless stated otherwise, the initial population size will be used as the
 99 reference population size in the various numerical examples. In the diffusion limit, the relative
 100 population size $N(t)/N_{\text{ref}}$ converges to a scaling function which we denote by $\rho(t)$.

101 We assume the infinitely-many-sites model (Kimura 1969) with A_0 and A_1 denoting the ances-
 102 tral and derived allelic types, respectively. The relative fitnesses of A_1/A_1 and A_1/A_0 genotypes
 103 over the A_0/A_0 genotype are respectively given by $1 + 2s$ and $1 + s$. The population-scaled selection
 104 coefficient is denoted by $\sigma = 2N_{\text{ref}} \cdot s$. The frequency of the derived allele A_1 at time t is denoted
 105 by X_t . Let f be a twice continuously differentiable, bounded function over $[0, 1]$. The backward
 106 generator of a time-inhomogeneous one-dimensional WF diffusion process on $[0, 1]$ is denoted by
 107 \mathcal{L} , which acts on f as

$$\mathcal{L}f(x) = \frac{1}{2}b(x; t)\frac{\partial^2}{\partial x^2}\{f(x)\} + a(x)\frac{\partial}{\partial x}\{f(x)\}, \quad (1)$$

108 where the diffusion and drift terms are given by $b(x; t) = x(1 - x)/\rho(t)$ and $a(x) = \sigma x(1 - x)$,
 109 respectively. The dependence of the diffusion term on time introduces considerable challenges
 110 to obtaining analytic results. To gain insights, we here focus on the case where ρ is piecewise
 111 constant. In this case, the diffusion and drift terms differ by a constant factor within each piece,
 112 thus simplifying the analysis.

113 Throughout, we assume that ρ has K constant pieces (or epochs) in the time interval $[\tau_0, \tau)$.
 114 The change points are denoted by t_1, \dots, t_{K-1} , and for convenience we define $t_0 = \tau_0$ and $t_K = \tau$.
 115 Then, for $t_i \leq t < t_{i+1}$, with $0 \leq i \leq K - 1$, we assume $\rho(t) = c_i$, where c_i is some positive
 116 constant. For the epoch $t_i \leq t < t_{i+1}$, the diffusion term is thus given by $b(x) = x(1 - x)/c_i$ and the
 117 corresponding generator is denoted by \mathcal{L}^i . The scale density ξ_i (Karlin and Taylor 1981, Ch. 15)
 118 for the epoch is given by

$$\xi_i(x) = \exp\left[-\int_0^x \frac{2a(z)}{b(z)} dz\right] = \exp(-2c_i \sigma x),$$

119 while the speed density π_i is given (up to a constant) by

$$\pi_i(x) = [b(x)\xi_i(x)]^{-1} = \frac{c_i \exp(2c_i\sigma x)}{x(1-x)}. \quad (2)$$

120 Given real-valued functions f and g on $[0, 1]$ that satisfy appropriate boundary conditions and
 121 are square integrable with respect to some real positive density h , we use $\langle f, g \rangle_h$ to denote

$$\langle f, g \rangle_h = \int_0^1 f(x)g(x)h(x)dx.$$

122 **The transition density within each epoch** $[t_i, t_{i+1})$

123 For the epoch $[t_i, t_{i+1})$, let the transition density be denoted by $p_i(t; x, y)$, where $t \in [t_i, t_{i+1})$,
 124 $X_{t_i} = x$ and $X_t = y$. Under the initial condition $p_i(t_i; x, y) = \delta(x - y)$, the spectral representation
 125 of $p_i(t; x, y)$ is given by

$$p_i(t; x, y) = \sum_{n=0}^{\infty} \exp[-\Lambda_n^i(t - t_i)] \pi_i(y) \Phi_n^i(x) \Phi_n^i(y) \frac{1}{\langle \Phi_n^i, \Phi_n^i \rangle_{\pi_i}}, \quad (3)$$

126 where $-\Lambda_n^i$ and Φ_n^i are the eigenvalues and eigenfunctions of \mathcal{L}^i , respectively. That is,

$$\mathcal{L}^i \Phi_n^i(x) = -\Lambda_n^i \Phi_n^i(x).$$

127 It can be shown that the eigenvalues are all real and non-positive. Furthermore,

$$0 \leq \Lambda_0^i < \Lambda_1^i < \Lambda_2^i < \dots,$$

128 with $\Lambda_n^i \rightarrow \infty$ as $n \rightarrow \infty$. The associated eigenfunctions $\{\Phi_n^i(x)\}_{n=0}^{\infty}$ form an orthogonal basis of
 129 $L^2([0, 1], \pi_i)$, the space of real-valued functions on $[0, 1]$ that are square integrable with respect to
 130 the speed density π_i , defined in (2).

131 Song and Steinrücken (2012) recently developed a method for finding Λ_n^i and Φ_n^i in the case
 132 of $c_i = 1$. We will give a brief description of their method and modify it accordingly to incorporate
 133 an arbitrary $c_i > 0$. Let \mathcal{L}_0^i denote the diffusion generator under neutrality (i.e., $\sigma = 0$). The
 134 eigenfunctions of \mathcal{L}_0^i are modified Gegenbauer polynomials $\{G_n(x)\}_{n=0}^{\infty}$ (cf. *Appendix*), and the

135 corresponding eigenvalues are $-\lambda_n^i$, with

$$\lambda_n^i = \binom{n+2}{2} \frac{1}{c_i}. \quad (4)$$

136 Similar to Song and Steinrücken (2012), define $H_n^i(x)$ as

$$H_n^i(x) = \frac{\exp(-c_i \sigma x)}{\sqrt{c_i}} G_n(x). \quad (5)$$

137 Then, $\{H_n^i(x)\}_{n=0}^\infty$ form an orthogonal system with respect to the weight function $\pi_i(x)$. By directly
 138 applying the full generator \mathcal{L}^i to $H_n^i(x)$, we observe that $H_n^i(x)$ are not eigenfunctions of \mathcal{L}^i .
 139 Instead, we obtain

$$\mathcal{L}_i H_n^i(x) = -[\lambda_n^i + c_i Q(x; \sigma)] H_n^i(x), \quad (6)$$

140 where $Q(x; \sigma) = 1/2 \cdot \sigma^2 x(1-x)$. However, since both $\{H_n^i(x)\}_{n=0}^\infty$ and $\{\Phi_n^i(x)\}_{n=0}^\infty$ are orthogonal
 141 with respect to the same weight function $\pi_i(x)$, and $\{H_n^i(x)\}_{n=0}^\infty$ form a basis of $L^2([0, 1], \pi_i)$, we
 142 can represent $\Phi_n^i(x)$ as a linear combination of $H_m^i(x)$:

$$\Phi_n^i(x) = \sum_{m=0}^\infty u_{n,m}^i H_m^i(x). \quad (7)$$

143 Furthermore, the fact that $\Phi_n^i(x)$ is an eigenfunction of \mathcal{L}^i with eigenvalue $-\Lambda_n^i$ implies that
 144 $\{u_{n,m}^i\}_{m=0}^\infty$ and Λ_n^i satisfy the following equation:

$$\begin{pmatrix} \lambda_0^i + c_i a_0^{(0)} & 0 & c_i a_2^{(-2)} & 0 & 0 & \cdots \\ 0 & \lambda_1^i + c_i a_1^{(0)} & 0 & c_i a_3^{(-2)} & 0 & \cdots \\ c_i a_0^{(+2)} & 0 & \lambda_2^i + c_i a_2^{(0)} & 0 & c_i a_4^{(-2)} & \cdots \\ 0 & c_i a_1^{(+2)} & 0 & \lambda_3^i + c_i a_3^{(0)} & 0 & \cdots \\ 0 & 0 & c_i a_2^{(+2)} & 0 & \lambda_4^i + c_i a_4^{(0)} & \cdots \\ \vdots & \vdots & \vdots & \vdots & \vdots & \ddots \end{pmatrix} \begin{pmatrix} u_{n,0}^i \\ u_{n,1}^i \\ u_{n,2}^i \\ u_{n,3}^i \\ u_{n,4}^i \\ \vdots \end{pmatrix} = \Lambda_n^i \begin{pmatrix} u_{n,0}^i \\ u_{n,1}^i \\ u_{n,2}^i \\ u_{n,3}^i \\ u_{n,4}^i \\ \vdots \end{pmatrix}, \quad (8)$$

145 where λ_n^i is as defined in (4) and $a_m^{(-2)}, a_m^{(0)}, a_m^{(+2)}$ are known constants that depend on σ and m
 146 (cf. Song and Steinrücken 2012 for details).

147 The transition density expansion (3) can be obtained by numerically solving the eigensys-

148 tem (8). Denote the infinite-dimensional matrix on the left hand side of (8) by W_i . The eigenval-
 149 ues Λ_n^i of W_i correspond (up to a sign) to the eigenvalues of \mathcal{L}^i , and the associated eigenvectors
 150 $\mathbf{u}_n^i = (u_{n,0}^i, u_{n,1}^i, u_{n,2}^i, \dots)^T$ of W_i determine the eigenfunctions of \mathcal{L}^i via (7). Let $W_i^{[D]}$ denote
 151 the $D \times D$ matrix obtained by taking the first D rows and D columns of W_i , and let $\Lambda_n^{i,[D]}$ and
 152 $\mathbf{u}_n^{i,[D]} = (u_{n,0}^{i,[D]}, u_{n,1}^{i,[D]}, u_{n,2}^{i,[D]}, \dots)^T$ denote the eigenvalues and eigenvectors of $W_i^{[D]}$, respectively.
 153 The truncated eigensystem

$$W_i^{[D]} \mathbf{u}_n^{i,[D]} = \Lambda_n^{i,[D]} \mathbf{u}_n^{i,[D]} \quad (9)$$

154 can then be used to approximate (8). This finite-dimensional linear system can be easily solved
 155 numerically. Since the truncated versions of the eigenvalues and eigenvectors converge rapidly as
 156 D increases, an accurate approximation of the transition density (3) can be efficiently obtained.
 157 The rapid convergence behavior of the eigenvalues is illustrated in Figure 1. As one would expect,
 158 the truncation level D required for convergence is higher when modeling a large population (cf.
 159 Figure 1b) compared to the basic selection model (cf. Figure 1a), while convergence is fast in
 160 a model with smaller population size (cf. Figure 1c). This is because the necessary truncation
 161 level correlates with the effective strength of selection, which is higher in large populations and
 162 lower in small populations. Therefore, for a fixed selection coefficient s , large populations are
 163 computationally more demanding than small populations.

164 **The transition density for the entire period $[\tau_0, \tau)$ with K epochs**

165 Suppose $X_{\tau_0} = x$ and $X_{\tau} = y$. The transition density $p(\tau_0, \tau; x, y)$ for the entire period $[\tau_0, \tau)$ is
 166 obtained by combining the transition densities for the K epochs as follows:

$$p(\tau_0, \tau; x, y) = \int_{[0,1]^{K-1}} p_0(t_1; x, x_1) \left[\prod_{i=1}^{K-2} p_i(t_{i+1}; x_i, x_{i+1}) \right] p_{K-1}(\tau; x_{K-1}, y) dx_1 \dots dx_{K-1}, \quad (10)$$

167 where x_i denotes the allele frequency at the change point t_i . Using (3), we can write (10) as

$$p(\tau_0, \tau; x, y) = \Phi_0(x)^T \mathbf{E}_0 \mathbf{S}_0 \mathbf{E}_1 \mathbf{S}_1 \cdots \mathbf{E}_{K-2} \mathbf{S}_{K-2} \mathbf{E}_{K-1} \Phi_{K-1}(y) \pi_{K-1}(y), \quad (11)$$

168 where $\Phi_i(x) = (\Phi_0^i(x), \Phi_1^i(x), \Phi_2^i(x), \dots)^T$ is an infinite-dimensional column vector, while E_i and
 169 S_i are infinite-dimensional matrices defined as

$$E_i = \text{diag} \left(\frac{e^{-\Lambda_0^i(t_{i+1}-t_i)}}{\langle \Phi_0^i, \Phi_0^i \rangle_{\pi_i}}, \frac{e^{-\Lambda_1^i(t_{i+1}-t_i)}}{\langle \Phi_1^i, \Phi_1^i \rangle_{\pi_i}}, \dots \right)$$

170 and

$$S_i = \int_0^1 \pi_i(z) \Phi_i(z) \Phi_{i+1}(z)^T dz.$$

171 In general, S_i is not a diagonal matrix since $\Phi_n^i(z)$ and $\Phi_m^{i+1}(z)$ are not orthogonal with respect to
 172 $\pi_i(z)$ if $c_i \neq c_{i+1}$. In the *Appendix*, we show that the entry (n, m) of S_i is given by

$$\begin{aligned} \int_0^1 \pi_i(z) \Phi_n^i(z) \Phi_m^{i+1}(z) dz &= \sqrt{\frac{c_i}{c_{i+1}}} \sum_{k=0}^{\infty} \sum_{l=0}^{\infty} u_{n,k}^i u_{m,l}^{i+1} \sum_{j=1}^{k+l+2} (-1)^{j+1} \frac{e^{\sigma(c_i - c_{i+1})} - (-1)^{k+l+j}}{[\sigma(c_i - c_{i+1})]^{j+1}} \\ &\times \frac{(k+1)(l+1)j!}{(k+2)(l+2)} \sum_{r=0}^{j-1} \binom{k+2}{j-r} \binom{k+j-r}{j-r-1} \binom{l+r+2}{r+1} \binom{l}{r}. \end{aligned} \quad (12)$$

173 Note that the last line of (12) does not depend on n or m , so it needs to be computed only once.
 174 The overall computational time for evaluating $p(\tau_0, \tau; x, y)$ scales linearly with the number K of
 175 epochs.

176 To better understand the joint impact of selection and demography on the transition density
 177 function, we consider two scenarios, where $p(0, \tau; x, y)$ is simply denoted as $p(\tau; x, y)$. Figure 2
 178 illustrates the density in a scenario in which the selection coefficient is fixed and various K -epoch
 179 demographic models are considered. In comparison to the case of a constant population size (cf.
 180 Figure 2a), an instantaneous expansion (cf. Figure 2b) narrows the distribution around the mean,
 181 whereas an additional phase of a reduced population size (cf. Figure 2c) increases the variance
 182 relative to a population of a constant size. Figure 3 illustrates the same scenarios with a fixed
 183 transition time and varying selection coefficients.

184 The sample frequency spectrum (SFS)

185 The transition density function approach

186 The transition density function derived in the previous section can be employed to obtain the SFS
 187 of a sample. Consider a sample of size n obtained at time $t = \tau$. The probability that the A_1 allele

188 with frequency x at time $t = \tau_0$ is observed b times in the sample is (Griffiths 2003)

$$p_{n,b}(x; \tau_0, \tau) = \int_0^1 \binom{n}{b} y^b (1-y)^{n-b} p(\tau_0, \tau; x, y) dy. \quad (13)$$

189 For piecewise-constant population size models with K epochs, a spectral representation of
 190 $p(\tau_0, \tau; x, y)$ can be found via (11) and evaluating (13) involves computing the integral
 191 $\int_0^1 y^b (1-y)^{n-b} \pi_{K-1}(y) \Phi_{K-1}(y) dy$. For $l \geq 0$, using (2), (5), and (7), we obtain

$$\begin{aligned} & \int_0^1 y^b (1-y)^{n-b} \pi_{K-1}(y) \Phi_l^{K-1}(y) dy \\ &= \sum_{m=0}^{\infty} \sqrt{c_{K-1}} u_{l,m}^{K-1} \int_0^1 y^{b-1} (1-y)^{n-b-1} e^{c_{K-1} \cdot \sigma y} G_m(y) dy \\ &= \sum_{m=0}^{\infty} \sqrt{c_{K-1}} u_{l,m}^{K-1} \frac{1}{b+1} \sum_{h=0}^m (-1)^{h+1} \frac{\binom{m+1}{h+1} \binom{h+m+2}{h}}{\binom{n+h+1}{b+1}} \cdot {}_1F_1(b+1; n+h+2; c_{K-1} \cdot \sigma), \quad (14) \end{aligned}$$

192 where ${}_1F_1(a; b; z) = \sum_{j \geq 0} a_{(j)} / b_{(j)} z^j / j!$ is the confluent hypergeometric function of the first kind. The
 193 descending factorials $d_{(j)}$ are defined in the *Appendix*.

194 The sample frequency spectrum (SFS) $q_{n,b}(\tau)$ is the probability distribution on the number b of
 195 mutant alleles in a sample of size n taken at time τ , conditioned on segregation. For $1 \leq b \leq n-1$,
 196 $q_{n,b}(\tau)$ is given by

$$q_{n,b}(\tau) = \lim_{x \rightarrow 0} \frac{\int_{-\infty}^{\tau} p_{n,b}(x; \tau_0, \tau) d\tau_0}{\int_{-\infty}^{\tau} \sum_{a=1}^{n-1} p_{n,a}(x; \tau_0, \tau) d\tau_0}. \quad (15)$$

197 In (15), the SFS at a single site is obtained by averaging over sample paths. This is equivalent
 198 to the frequency spectrum distribution over a large number of independent mutant sites in the
 199 Poisson random field model of Sawyer and Hartl (1992). Using (11), (12), (13), and (14), we can
 200 approximate (15) numerically. If it is unknown which allele is derived, a folded version of (15) can
 201 be obtained as $[q_{n,b} + q_{n,n-b}] / (1 + \delta_{b,n-b})$, where $\delta_{b,n-b}$ denotes the Kronecker delta.

202 A method of moment approach

203 As detailed above, the transition density function can be employed to obtain the SFS. However,
 204 the specific solution for the transition density is not required to obtain the less complex and thus
 205 computationally less demanding SFS. Here, we utilize the work of Evans et al. (2007) to develop

206 an efficient algorithm for computing the allele frequency spectrum in the case of genic selection
 207 and piecewise-constant population sizes.

208 Suppose mutations arise at rate $\theta/2$ (per sequence per $2N_{\text{ref}}$ generations) and according to the
 209 infinitely-many-sites model (Kimura 1969). Evans et al. (2007) use the forward diffusion equation
 210 to describe population allele frequency changes and introduce mutations by an appropriate bound-
 211 ary condition. Slightly modifying their notation, we use $f(y, t)dy$ to denote the expected number of
 212 sites where the mutant allele has a frequency in $(y, y + dy)$, with $0 < y < 1$, at time t . The forward
 213 equation is

$$\frac{\partial}{\partial t}f(y, t) = \frac{1}{2} \frac{\partial^2}{\partial y^2} \{b(y; t)f(y, t)\} - \frac{\partial}{\partial y} \{a(y)f(y, t)\}, \quad (16)$$

214 where the diffusion term $b(y; t) = y(1 - y)/\rho(t)$, the drift term $a(y) = \sigma y(1 - y)$, the scaled selection
 215 coefficient σ , and the population size function $\rho(t)$ are defined as before. The influx of mutations
 216 is incorporated into this process via the boundary conditions

$$\lim_{y \downarrow 0} yf(y, t) = \theta\rho(t) \quad \text{and} \quad \lim_{y \uparrow 1} f(y, t) \text{ finite.} \quad (17)$$

217 The resulting polymorphic sites follow the dynamics of (16) thereafter. Note that this differs from
 218 the diffusion process studied in the previous section, as the influx of mutations is now explicitly
 219 modeled.

220 Again, it is analytically more practical to consider the corresponding backward equation, which
 221 is obtained by setting $g(y, t) := y(1 - y)f(y, t)$. This substitution transforms the forward equation
 222 for $f(y, t)$ into a backward equation for $g(y, t)$, which is essentially given by (1) up to the sign of the
 223 drift term. Evans et al. (2007) derived a coupled system of ordinary differential equations (ODEs)
 224 for the moments $\mu_j(t) = \int_0^1 y^j g(y, t) dy$:

$$\mu'_0(t) = \frac{\theta}{2} - \frac{1}{\rho(t)}\mu_0(t) + \sigma[\mu_0(t) - 2\mu_1(t)], \quad (18)$$

$$\begin{aligned} \mu'_j(t) = \frac{1}{\rho(t)} \left[\binom{j+1}{2} \mu_{j-1}(t) - \binom{j+2}{2} \mu_j(t) \right] + \\ \sigma \left[(j+1)\mu_j(t) - (j+2)\mu_{j+1}(t) \right], \quad j \geq 1, \end{aligned} \quad (19)$$

225 where $\mu'_j(t) = d\mu_j(t)/dt$. A similar system of ODEs was derived and solved by Kimura (1955a) for
 226 a neutral scenario with a constant population size and without mutations. For $\sigma = 0$, the above

227 system is finite and can be solved explicitly (Živković and Stephan 2011). In the case of selection
 228 ($\sigma \neq 0$), on the other hand, the system is infinite and obtaining an explicit solution for an arbitrary
 229 ρ is a challenging problem, even if the system is truncated by setting $\mu_j(t) = 0$ for $j \geq D$.

230 From now on, assume $\mu_j(t) \equiv 0$ for $j \geq D$ and rewrite the truncated system of ODEs in matrix
 231 form as

$$M'(t) = \left[\frac{1}{\rho(t)} \mathbf{B} + \sigma \mathbf{A} \right] M(t) + \Theta, \quad (20)$$

232 where $M(t) = (\mu_0^{[D]}(t), \mu_1^{[D]}(t), \dots, \mu_{D-1}^{[D]}(t))^T$, $M'(t) = dM(t)/dt$, $\Theta = (\theta/2, 0, \dots, 0)^T$ are D -
 233 dimensional column vectors, and $\mathbf{B} = (b_{kl})$ and $\mathbf{A} = (a_{kl})$ are $D \times D$ matrices with entries

$$b_{kl} = \begin{cases} -\binom{k+2}{2}, & \text{if } l = k, \\ \binom{k+1}{2}, & \text{if } l = k - 1, \\ 0, & \text{otherwise,} \end{cases} \quad \text{and} \quad a_{kl} = \begin{cases} k + 1, & \text{if } l = k, \\ -(k + 2), & \text{if } l = k + 1, \\ 0, & \text{otherwise,} \end{cases}$$

234 for $0 \leq k, l \leq D - 1$. The formal solution of (20) cannot be written in terms of a matrix exponential
 235 but only as a Peano-Baker series (Baake and Schlägel 2011) for arbitrary ρ , which can be numer-
 236 ically quite demanding. Therefore, we focus on the case of piecewise constant ρ and develop an
 237 efficient method to solve the truncated system of ODEs.

238 We first consider $\rho(t) \equiv c_0$ (i.e., a constant population size), for which the solution of (20) takes
 239 the form of a matrix exponential given by

$$\begin{aligned} M(t) &= \exp \left[\int_0^t \left(\frac{\mathbf{B}}{c_0} + \sigma \mathbf{A} \right) ds \right] M(0) + \left\{ \int_0^t \exp \left[\int_s^t \left(\frac{\mathbf{B}}{c_0} + \sigma \mathbf{A} \right) du \right] ds \right\} \Theta \\ &= \exp \left[\left(\frac{\mathbf{B}}{c_0} + \sigma \mathbf{A} \right) t \right] M(0) + \left\{ \exp \left[\left(\frac{\mathbf{B}}{c_0} + \sigma \mathbf{A} \right) t \right] - \mathbf{I} \right\} \left(\frac{\mathbf{B}}{c_0} + \sigma \mathbf{A} \right)^{-1} \Theta. \end{aligned} \quad (21)$$

240 Let $-\lambda_k, (l_{k,0}, \dots, l_{k,D-1})$, and $(r_{0,k}, \dots, r_{D-1,k})^T$ respectively denote the eigenvalues, row eigen-
 241 vectors, and column eigenvectors of $\mathbf{B}/c_0 + \sigma \mathbf{A}$. Then, (21) implies

$$\mu_j^{[D]}(t) = \sum_{i=0}^{D-1} \mu_i^{[D]}(0) \sum_{k=0}^{D-1} r_{jk} l_{ki} e^{-\lambda_k t} + \frac{\theta}{2} \sum_{k=0}^{D-1} r_{jk} l_{k0} \frac{1 - e^{-\lambda_k t}}{\lambda_k}. \quad (22)$$

242 It is intractable to find closed-form expressions of $-\lambda_k, l_{ki}$, and r_{jk} , but, for a given truncation level

243 D , they can be computed numerically. Depending on the details of the model under consideration,
 244 it might be more efficient to solve (21) numerically rather than applying the more analytic form
 245 given in (22).

246 We now investigate the equilibrium solution of (22), since it can be applied as an initial condi-
 247 tion in a model in which the population size remains constant over a longer period of time before
 248 instantaneous population size changes occur. Assuming that all alleles are monomorphic at time
 249 zero, i.e. $\mu_i^{[D]}(0) \equiv 0$, and letting $t \rightarrow \infty$, we obtain the moments at equilibrium as

$$\hat{\mu}_j^{[D]} = \frac{\theta}{2} \sum_{k=0}^{D-1} \frac{r_{jk} l_{k0}}{\lambda_k}.$$

250 For D sufficiently large, this result is numerically close to the exact solution $\hat{\mu}_j$. The latter can also
 251 be obtained as follows. The equilibrium population frequency spectrum is given by (Fisher 1930)

$$\hat{f}(y) = \frac{\theta c_0 [1 - e^{-2c_0\sigma(1-y)}]}{y(1-y)(1 - e^{-2c_0\sigma})}. \quad (23)$$

252 The sampled version can be easily found via binomial sampling as in (13):

$$\hat{f}_{n,b} = \theta c_0 \frac{n}{b(n-b)} \frac{1 - {}_1F_1(b; n; 2c_0\sigma)e^{-2c_0\sigma}}{1 - e^{-2c_0\sigma}}. \quad (24)$$

253 For $\sigma \neq 0$, the moments $\hat{\mu}_j$ of $\hat{g}(y) = y(1-y)\hat{f}(y)$ are given by

$$\hat{\mu}_j = \theta c_0 \frac{1}{1 - e^{-2c_0\sigma}} \left\{ \frac{e^{-2c_0\sigma} [\Gamma(j+1, -2c_0\sigma) - j!]}{(-2c_0\sigma)^{j+1}} + \frac{1}{j+1} \right\},$$

254 where $\Gamma(a, z) = \int_z^\infty t^{a-1} e^{-t} dt$ is the incomplete gamma function.

255 Now, consider the piecewise-constant model with K epochs in the time interval $[\tau_0, \tau]$ defined
 256 earlier. For $t_i \leq t < t_{i+1}$,

$$\mathbf{M}'(t) = \left(\frac{\mathbf{B}}{c_i} + \sigma \mathbf{A} \right) \mathbf{M}(t) + \Theta, \quad (25)$$

257 which can be solved as in (21). For $\tau > t_{K-1}$,

$$\begin{aligned} \mathbf{M}(\tau) = & \exp \left[\left(\frac{\mathbf{B}}{c_{K-1}} + \sigma \mathbf{A} \right) (\tau - t_{K-1}) \right] \mathbf{M}(t_{K-1}) + \\ & \left\{ \exp \left[\left(\frac{\mathbf{B}}{c_{K-1}} + \sigma \mathbf{A} \right) (\tau - t_{K-1}) \right] - \mathbf{I} \right\} \left(\frac{\mathbf{B}}{c_{K-1}} + \sigma \mathbf{A} \right)^{-1} \Theta, \end{aligned} \quad (26)$$

258 where $M(t_i)$, for $1 \leq i \leq K - 1$, is recursively given by

$$M(t_i) = \exp \left[\left(\frac{\mathbf{B}}{c_{i-1}} + \sigma \mathbf{A} \right) (t_i - t_{i-1}) \right] M(t_{i-1}) + \left\{ \exp \left[\left(\frac{\mathbf{B}}{c_{i-1}} + \sigma \mathbf{A} \right) (t_i - t_{i-1}) \right] - \mathbf{I} \right\} \left(\frac{\mathbf{B}}{c_{i-1}} + \sigma \mathbf{A} \right)^{-1} \Theta.$$

259 The initial condition $M(t_0)$ is either chosen as the equilibrium solution described above or the zero
260 vector, which corresponds to the case of all loci being monomorphic at time $t_0 = \tau_0$.

261 The accuracy of the above framework depends on how fast the truncated moments $\mu_j^{[D]}(\tau)$ con-
262 verge to zero as D increases. In general, the truncated moments converge faster for negative than
263 for positive σ , and for instantaneous declines compared to instantaneous expansions (cf. Figure 4).
264 For a large positive σ , a higher truncation level D may be required to achieve the desired accuracy.
265 Finally, the allelic spectrum $f_{n,b}(\tau)$, for $1 \leq b \leq n - 1$, of a sample of size n taken at time τ can be
266 obtained from the moments $\mu_j(\tau)$ via (26) and by using the relationship

$$f_{n,b}(\tau) = \binom{n}{b} \sum_{l=0}^{n-b-1} (-1)^l \binom{n-b-1}{l} \mu_{l+b-1}(\tau). \quad (27)$$

267 The SFS $q_{n,b}(\tau)$ at time τ is then given by

$$q_{n,b}(\tau) = \frac{f_{n,b}(\tau)}{\sum_{a=1}^{n-1} f_{n,a}(\tau)}. \quad (28)$$

268 The joint impact of a population bottleneck and selection on the SFS is illustrated in Figure 5
269 for various points in time. As expected, negative and positive selection result in a skew of the SFS
270 towards low- and high-frequency derived variants, respectively, when compared to a model without
271 selection, across all sampling times. Moreover, this skew varies in intensity at different points in
272 time. In the neutral demographic model (cf. Figure 5b), the relative frequency of singletons at time
273 τ_3 is higher than at time τ_4 , whereas under the same demographic model with negative selection
274 (cf. Figure 5c) this relation is inverted. This is because the amount of singletons that is caused
275 by demographic forces decreases after the expansion from τ_3 to τ_4 , while negative selection is still
276 increasing the low-frequency derived classes in this time interval.

Applications

277

278 Here, we discuss some biologically relevant questions that can be addressed using our theoretical
279 framework. This section consists of the following three parts:

- 280 1. We first consider models with negative selection and bottlenecks of medium strength at differ-
281 ent time points. We examine the SFS under such models and try to estimate the demographic
282 parameters while taking selection into account. We also carry out demographic inference
283 while ignoring selection. Whereas the former demonstrates how well the demographic and
284 selective parameters can be estimated jointly, the latter mimics the common practice of as-
285 suming genome-wide polymorphic sites as putatively neutral (due to the difficulty of jointly
286 estimating the impact of selection and demography using existing tools). We finally examine
287 the consequences of assuming a too simple underlying demography on parameter estimation.
- 288 2. We then analyze an African sample of *Drosophila melanogaster* to investigate its demographic
289 history and possible selective effects.
- 290 3. Lastly, we examine a model of strong exponential population growth (mimicking human evo-
291 lution) and superimpose negative selection of various strengths to understand if and when
292 selection can be inferred for such a model.

293 Throughout, the first population size change will occur after the allele frequencies have reached an
294 equilibrium according to (24).

295 **Joint inference of population bottleneck and purifying selection**

296 *A maximum likelihood approach*

297 Under the assumption that the considered sites are independent, the log-likelihood of a model
298 \mathcal{M} given data \mathcal{D} is $\log[L(\mathcal{D}; \mathcal{M})] = \sum_{i=1}^{n-1} d_i \log(q_i) + \text{constant}$, where d_i is the observed number
299 of sites at which the derived allele occurs i times in the sample, and q_i is the probability that the
300 derived allele occurs i times in the sample at a segregating site under model \mathcal{M} (e.g., Wooding
301 and Rogers 2002). Recall that q_i can be either obtained via the transition density function or the
302 method of moment approach.

303 Consider the bottleneck model illustrated in Figure 6. Note that the present relative size c_S is
304 fixed to 1, i.e., here the present population size is used as the reference population size N_{ref} . First,
305 we consider the scenario where the ancestral population size c_0 prior to the bottleneck is allowed

306 to vary. In this case, the model has five free parameters: c_0 , the initial population size; c_B , the
307 population size during the bottleneck; t_B , the duration of the bottleneck; $t_S = \tau - t_B$, the time
308 since recovery from the bottleneck; and σ , the scaled selection coefficient. We then also consider
309 the scenario where the ancestral population size is the same as the present population size, i.e.,
310 $c_0 = c_S$, resulting in a model with four free parameters.

311 We adopted a grid search in our estimation procedure, with $\sigma \in [-10, 0]$ and $c_B, t_B, t_S \in$
312 $[0.001, 1]$. For the 5-parameter model, c_0 was chosen from the range $[0.01, 10]$. In total, 110,000
313 grid points were chosen in the selected case and 10,000 in the neutral case. Note that the grid
314 search also accounts for models of one or two successive instantaneous population expansions. For
315 the 4-parameter model, 11,000 grid points were chosen in the selected case and 1000 in the neutral
316 case. The grid points are summarized in Table 1.

317 *Estimation of bottleneck and selection parameters*

318 We first evaluated the SFS for a sample of size $n = 50$ in the following twelve scenarios, all with
319 $c_S = 1$ and $\sigma \in \{0, -1/2, -2\}$:

- 320 1. Constant population size (i.e., $c_0 = c_B = c_S = 1$).
- 321 2. Bottleneck models with $c_0 = 1/2, c_B = 1/10, t_B = 1/10$, and $t_S \in \{1/200, 1/20, 1/2\}$.

322 First, to test how well the demographic and selective parameters can be estimated jointly from
323 sampled data, we focused on the bottleneck demography with $t_S = 1/20$ and considered two
324 scenarios: The neutral case ($\sigma = 0$) and the selected case with $\sigma = -2$. To mimic the limited avail-
325 ability of independent polymorphic sites across the genome, we sampled 10,000 sites according to
326 the SFS for the two chosen scenarios, and repeated this procedure 200 times. For each of these
327 200 datasets, we maximized the log-likelihood over the grid of parameter values described earlier,
328 assuming (A1) neutrality when the true model has $\sigma = 0$, (A2) neutrality when the true model
329 has $\sigma = -2$, (A3) presence of selection when the true model has $\sigma = -2$, and (A4) presence of
330 selection when the true model has $\sigma = 0$.

331 The estimated parameters are shown in Table 2. For inference under correct model assumptions
332 (A1 and A3), the median estimates are equal to the true parameters. When selection is ignored
333 although present in the dataset (A2), the ancestral population size (\hat{c}_0) and the duration of the bot-
334 tleneck (\hat{t}_B) are underestimated, whereas the bottleneck size (\hat{c}_B) and the time since the bottleneck
335 (\hat{t}_S) are accurately estimated. When the true model is neutral but the inference procedure allows
336 for selection (A4), a neutral demographic model is accurately inferred. We calculated likelihood-

337 ratio statistics for each of the 200 datasets to compare the two nested models of selection and
338 neutrality. The null hypothesis of neutrality can be rejected at the 5% significance level with a
339 power of 55%.

340 We further analyzed all twelve scenarios using the expected SFS directly, assuming that the
341 amount of data is sufficiently large such that the observed SFS has converged to the expected
342 value. Our goal in this case is to study the effect of model misspecification on parameter estimation;
343 specifically, assuming selection when the true model is neutral or assuming neutrality when there
344 is selection. In the former case, the maximum likelihood estimates always coincided with the
345 true parameters. Therefore, it is useful to allow for selection in an analysis even when putatively
346 neutral regions are considered. In the latter case, our results are summarized in Table 3. For a
347 constant population size, two rather old instantaneous expansions are estimated. For the bottleneck
348 models, ignoring selection leads to the largest errors for the most recent bottleneck and $\sigma = -1/2$
349 and the least recent bottleneck and $\sigma = -2$, for which an instantaneous expansion is estimated.
350 Interestingly, the time since the bottleneck was robustly estimated in many cases.

351 To assess the impact of assuming a slightly simplified model for parameter estimation, we car-
352 ried out an analogous study where the ancestral population size c_0 was incorrectly assumed to
353 equal the current size $c_S = 1$, while the true model had $c_0 = 1/2$ and $c_S = 1$. For the resampling
354 analysis, we considered the same bottleneck scenarios as before with $\sigma = 0$ or -2 , and maximized
355 the log-likelihood values over a grid in the parameter space (as described earlier) for each of the
356 200 simulated datasets each containing 10,000 polymorphic sites. The parameter estimates are
357 shown in Table 4. The time since the bottleneck (\hat{t}_S) is accurately estimated irrespective of correct
358 or wrong assumptions regarding selection. Incorrectly assuming $c_0 = c_S$ results in either an over-
359 estimation of the duration of the bottleneck (\hat{t}_B) in most of the cases (A1–A3) or an inference of
360 selection when $\sigma = 0$ (A4). Selection was poorly estimated even under (A3).

361 Again, we also analyzed all twelve scenarios under the assumption that the observed SFS has
362 converged to the expected value, to study the effect of model misspecification on parameter esti-
363 mation. The results are shown in Table 5. The biases caused by incorrectly assuming $c_0 = c_S$ are
364 largest for the scenario that captures the youngest bottleneck ($t_S = 1/200$). Here, not only the
365 selection coefficients are strongly misestimated but also the time since the bottleneck (\hat{t}_S) is largely
366 underestimated. In all the other scenarios, at least the time since the bottleneck (\hat{t}_S) is accurately
367 estimated. The estimation accuracy of the other demographic parameters and selection coefficient
368 increases with bottleneck age and the concomitant decreasing impact of the ancestral population

369 size on the SFS. In summary, we note that assuming a too simplistic demographic model can lead
370 to large errors in parameter estimation.

371 *Testing a dataset of *Drosophila melanogaster**

372 Here, we apply our method to analyze a dataset which has been recently used to estimate the
373 joint demographic history of several populations of *Drosophila melanogaster* (Duchen et al. 2013).
374 The dataset consists of 12 sequences from a Zimbabwe population comprising 197 non-coding loci;
375 and within each locus there are between 1 and 41 segregating sites (3234 polymorphic sites in
376 total). We carry out our analysis based on the bottleneck model of the previous section assuming
377 that the current and the ancestral population sizes are allowed to differ, assuming either neutrality
378 or selection on the derived variant. Since purifying selection is assumed to be more prevalent than
379 positive selection in intronic and intergenic regions of African *Drosophila*, we focus on a negative
380 selection coefficient in our analysis.

381 We primarily use all segregating sites in our analysis. However, whereas the loci are scattered
382 over the genome with at least tens of thousands of bases apart, the sites within each locus are
383 tightly linked and hence are not independent. To study the effect of this discrepancy between the
384 theoretical independence assumption underlying our method and the data, we also try using a
385 subset of presumably independent sites by sampling one from each locus.

386 To begin with, a coarse maximum likelihood estimate of $(\hat{c}_0, \hat{\sigma}, \hat{c}_B, \hat{t}_B, \hat{t}_S) = (1, 0, 0.05, 0.1, 0.1)$
387 was computed under the selective and the neutral bottleneck model on the parameter grid specified
388 earlier. For each model, we investigated the accuracy of this parameter estimate via parametric
389 bootstrap, using 200 bootstrap samples each consisting of 3234 polymorphic sites. Quantiles of the
390 MLEs from the bootstrap samples are shown in Table 6, and, e.g., the confidence interval of the
391 estimate of the ancestral population size (\hat{c}_0) spans nearly the entire given parameter range.

392 This suggests to improve the parameter estimates by successively refining the grid. The param-
393 eter range of each parameter was adjusted by choosing the respective two outermost parameter
394 estimates from the set of the 100 likeliest parameter combinations of the coarse grid. We fixed
395 the five possible ancestral population sizes $c_0 \in [0.5, 10]$ (cf. Table 1) occurring in this set, and
396 adopted a grid search for each of them, with $\sigma \in [-0.79, 0]$, $c_B \in [0.001, 0.1]$, $t_B/c_B \in [1, 5]$ and
397 $t_S \in [0.05, 0.224]$. Besides zero, 10 values were chosen for σ , 10 values for c_B , and 30 values each
398 for t_B/c_B and t_S , so that a total of 99,000 grid points were applied for each c_0 . The ratio of two
399 consecutive values in each parameter range is kept constant similarly to above. To focus on rescaled

400 time t_B/c_B instead of t_B relies on the observation that t_B and c_B correlate strongly and has the
401 advantage that unlikely combinations of t_B and c_B can be omitted. More values were chosen for
402 time parameters, since these are more sensitive than the population size parameters.

403 This procedure was repeated twice, upon which the maximum likelihood value did barely
404 change. Each refined grid was based on the 100 likeliest parameter estimates, and the number
405 of different possible ancestral population sizes was also successively raised to further refine the
406 parameter c_0 . The maximum likelihood estimates for a range of parameters c_0 and the associated
407 likelihoods are given in Table 7. Selection is barely needed to explain the dataset and the estimated
408 bottleneck population size (\hat{c}_B) has reached the smallest possible value of 0.001 over the various
409 grid searches. Choosing even distinctly smaller values for \hat{c}_B would barely change the likelihood
410 value anymore as long as the scaled bottleneck duration \hat{t}_B/\hat{c}_B is kept constant. The time since
411 the bottleneck (\hat{t}_S) is robustly estimated over the various demographies that provide a similar like-
412 lihood (L), whereas the estimated bottleneck duration (\hat{t}_B) correlates strongly with the ancestral
413 population size (c_0). Again, for each of the various ancestral population sizes (c_0), the set of the
414 100 likeliest parameter combinations was used to obtain the parameter and likelihood ranges pre-
415 sented in Table 8. As one can see, most parameters were sufficiently pinpointed. In Figure 7, the
416 SFS for the most likely neutral and selective parameter estimates, which can be found in the two
417 penultimate lines of Table 7, are compared with the observed data.

418 Comparing the SFS obtained using our parameter estimates and the ones given in Duchon
419 et al. (2013), we obtain an improved goodness-of-fit to the observed SFS from the data. This is not
420 surprising, since primarily statistics *summarizing* the SFS were used in their study. Furthermore, the
421 authors allowed for different population sizes before and after the bottleneck as well but restricted
422 the duration of the bottleneck to a somewhat arbitrary predefined value. The method in our work
423 does not take the mutation rate explicitly into account, and thus cannot estimate the reference
424 population size. Thus it would be too speculative to date the bottleneck in calendar time and to
425 compare our outcome to the estimate of Duchon et al.

426 To investigate the effect of linkage within each of the 197 sequence fragments in the original
427 dataset, we sampled one site per fragment to obtain a dataset consisting of 197 polymorphic sites.
428 We repeated this procedure 200 times and maximized the log-likelihood for each sample similarly
429 as above. Compared to the analysis of the full dataset, the SFS computed from the median pa-
430 rameter estimate shows a poorer fit to the data. This is likely due to the strong stochasticity in
431 the bootstrap resampling procedure, since the individual parameter estimates for each sample do

432 provide a good fit despite the small number of sites considered.

433 It might be tempting to assume that the excess of high-frequency derived variants in the ob-
434 served data might be a result of weak positive selection. Therefore, we conducted an equivalent
435 analysis as above, starting from the same grid with inverted signs for the selection coefficients.
436 However, we did not obtain estimates being plausible from a biological point of view, since the
437 estimation procedure favours selection coefficients in the upper range of the chosen interval $[0, 10]$.
438 When, as in this example, an excess of low- and high-frequency derived variants is simultaneously
439 observed in comparison to a standard neutral model, unrealistically large estimates for σ are needed
440 to explain the data. Positive selection on its own (and of some appreciable strength) causes a de-
441 cline of low-frequency derived variants and an excess of high-frequency derived alleles, whereas
442 an expansion (as embedded in the bottleneck model) acts vice versa. Therefore, both forces have
443 to severely counteract each other so that the requirements of both ends of the SFS can be met.

444 **A model of human exponential population growth**

445 We now demonstrate the utility of our method to investigate population size histories containing
446 epochs of exponential growth in combination with selection. To this end, we adopt the following
447 demographic history of a sample of African human exomes that has been estimated by Tennesen
448 et al. (2012) as a modification of a model by Gravel et al. (2011). The population had an ancestral
449 size of 7310 individuals until 5920 generations ago (assuming a generation time of 25 years),
450 when it increased instantaneously in size to 14,474 individuals. After this increase, the population
451 remained constant in size until 205 generations ago, when it started to grow exponentially until
452 reaching 424,000 individuals at present. The relative population size function for this model can
453 be described by

$$\rho(t) = \begin{cases} 1, & t < 0, \\ c, & 0 \leq t < t_e, \\ c \exp[R(t - t_e)], & t_e \leq t \leq \tau, \end{cases} \quad (29)$$

454 where c is the ratio of population sizes after and before the instantaneous expansion, which can be
455 dated arbitrarily, so we set the time of this expansion to zero. R is the scaled exponential growth
456 rate, t_e is the time at which the expansion started, and τ is the time of sampling (the present).
457 Times are given in units of $2N_{\text{ref}}$, where the reference population size N_{ref} is the initial size before

458 time zero (the ancestral size). Since the theoretical framework presented above assumes a history
459 of piecewise constant population sizes, the phase of exponential growth in this model has to be ade-
460 quately discretized to obtain a suitable piecewise approximation. The following piecewise function
461 can be chosen to approximate the exponential growth phase via a geometric growth function:

$$q(t) = \begin{cases} 1, & t < 0, \\ c, & 0 \leq t < t_1, \\ c(1 + \delta)^i, & t_i \leq t < t_{i+1}, \end{cases} \quad (30)$$

462 with times $t_i = t_e + \log [(1 + \delta)^{i-1}(2 + \delta)/2] / R$, $i = 1, \dots, i_\tau$. Here, the number of population size
463 changes during the phase of exponential growth is given by

$$i_\tau := \left\lfloor \frac{R(\tau - t_e) - \log(\delta/2 + 1)}{\log(\delta + 1)} \right\rfloor + 1.$$

464 Varying the growth rate δ determines the number of discretization intervals used.

465 The SFS (28) of the discretized version is obtained straightforwardly from (26) and (27). For
466 the demographic parameters given above, we computed the SFS for various sample sizes up to
467 200 and we used $\delta = 1/4$, which was chosen large enough to provide reasonable fast computation
468 times but sufficiently small to provide a good approximation of the exponential growth model. In
469 the neutral case, the goodness of the approximation can be verified via the explicit solution of
470 the SFS (Živković and Stephan 2011), which can be applied to the continuous and the discretized
471 model. As shown in Figure 8a, where a sample size of $n = 200$ is chosen, the spectra of both
472 continuous and piecewise-constant models agree very well with each other; the percentage error is
473 0.57% based on the l^2 -norm, while the Kullback-Leibler divergence is about 1.76×10^{-7} .

474 Using our method, selection can then be incorporated into the piecewise-constant population
475 size model. The effect of various negative selection coefficients (scaled with respect to the ancestral
476 population size) is illustrated again for sample size $n = 200$ in Figure 8b, and the same trend can
477 be observed for smaller sample sizes as well. It is probably not surprising that the resolution in
478 distinguishing the selective and the neutral model rises with σ . More interestingly, differences
479 between the neutral and the selective models are apparently more pronounced among derived
480 alleles in intermediate- to high frequency. Therefore, for large datasets where intermediate to high-
481 frequency derived alleles are present in sufficient numbers, one may focus more strongly on these
482 allelic classes than on low-frequency derived ones for the statistical analysis of purifying selection.

Discussion

483

484 Already in the early days of population genomics, several studies in various species (e.g., Glinka
485 et al. 2003, Williamson et al. 2005) have revealed that both natural selection and demographic
486 forces have shaped the patterns of polymorphism in modern samples of DNA sequences. However,
487 most inference methods relied on computer simulations and the usage of statistics that have been
488 designed to detect deviations from neutrality assuming a constant population size (e.g., Glinka
489 et al. 2003). More elaborate approaches utilized the transition density function that describes
490 allele frequency changes over time, where most methods solved the underlying diffusion equation
491 numerically employing discretization schemes (e.g., Williamson et al. 2005, Zhao et al. 2013).
492 Besides several issues that may arise in such purely numerical frameworks, only the simplest models
493 of a single population size change have been considered in these studies. Recently, Song and
494 Steinrücken (2012) developed a more analytical approach that provides the spectral representation
495 of the transition density for a model that includes general diploid selection and recurrent mutations
496 under a constant population size.

497 In this article, we extended their solution for the case of genic selection to an arbitrary number
498 of instantaneous changes in population size. First, we obtained a rescaled version of the spectral
499 representation of the transition density function for a single time period during which the popu-
500 lation size differs with respect to a reference size. Combining the transition densities for single
501 time periods over arbitrarily many time points of instantaneous population size changes yields the
502 transition density function for such a multi-epoch model with genic selection.

503 The transition density function has been employed to obtain the SFS. However, explicit knowl-
504 edge of the transition density function is not required for the computation of the SFS. We revisited
505 and simplified a method by Evans et al. (2007) who expressed the allele frequencies in terms of
506 their moments. Their method requires that a system of ordinary differential equations is solved nu-
507 merically. They employed a finite difference scheme to tackle a model of strong exponential growth
508 with genic selection. We simplified this approach starting from a model of a constant population
509 size, to which instantaneous population size changes were recursively added. The numerically
510 obtained result at the end of a certain epoch is used as the initial condition of the subsequent
511 time phase. This simple procedure allows us to consider numerous population size changes and
512 offers fast computations with little loss in accuracy. We have shown that even a model of strong
513 population growth can be well approximated.

514 The transition density function with variable population size can be incorporated into a hidden
515 Markov model framework (cf. Steinrücken et al. 2014 for a constant population size) to analyze
516 time series genetic data. However, in this article we focused on several biological questions that can
517 be investigated using the SFS, and treat the time series application in a separate paper. We first ad-
518 dressed the joint estimation of bottleneck and selection parameters from polymorphism data within
519 a maximum likelihood framework. This approach can be applied to *simultaneously* infer selection
520 coefficients and the parameters of a model of instantaneous population size changes. The impor-
521 tance of methods that allow to estimate selective and demographic parameters jointly becomes
522 particularly apparent in large populations for which the scaled selection coefficient, σ , can take
523 considerable values across large regions of the genome, so that demography and selection cannot
524 be estimated independently. Although selection is known to act either positively or negatively and
525 with different strengths across the genome, a constant selection coefficient has been applied in our
526 approach. A constant selection coefficient can either be interpreted as a genome-wide average, or,
527 more realistically, as the selection strength of a certain functional class, among which the coeffi-
528 cients should not vary greatly. This argument particularly applies to the *Drosophila* example for
529 which intronic and intergenic loci were sequenced and used for the parameter estimation.

530 For the first part of *Applications*, we generated data for the estimation procedure by sampling
531 a large number of sites from the SFS of a bottleneck model varying the strength of selection. We
532 assumed the same and also a slightly less complex model with five and four free parameters, re-
533 spectively, for the parameter estimation. We demonstrated that our method can accurately estimate
534 the parameters in the majority of the bottleneck scenarios, but less so, when the simpler model is
535 assumed. The time since the bottleneck was retrieved in most of the cases even when assuming the
536 simpler model. It is interesting to note that even when the datasets simulated with selection are an-
537 alyzed assuming neutrality, the time since the bottleneck was quite robustly inferred except for the
538 briefest one being estimated under the simpler 4-parameter model. This result is quite promising
539 with respect to the many published demographic estimates that have been obtained assuming neu-
540 trality, because the time since the last demographic change might not be subject to major changes.
541 However, this result has to be investigated further in more realistic models that also include phases
542 of exponential growth, which can be studied based on our results as well. Our results encourage
543 the application of rather complex than too simple demographic models anyway.

544 In the African *Drosophila* sample, no or barely any negative selection was inferred, which might
545 simply be a result of well chosen neutral markers that barely experienced selection. Furthermore,

546 it turned out to be difficult to pinpoint in particular the ancestral population size and the duration
547 of the bottleneck, whereas the time since the bottleneck was robustly estimated. From a theoretical
548 point of view, Bhaskar and Song (2014) have recently obtained sufficient conditions for the iden-
549 tifiability of piecewise-defined demographic models under neutrality using the expected frequency
550 spectrum; the identifiability of demographic models combined with selection is an interesting fu-
551 ture research question. However, one has to keep in mind that the estimates were obtained from
552 partly linked loci of a small sample of chromosomes and that taking a subset of independent loci to
553 meet the theoretical assumptions result in relatively small datasets showing large variance in the
554 estimates.

555 We finally analyzed an example of exponential human population growth (Tennessen et al.
556 2012) to see the effect of purifying selection in the context of this model. As illustrated in Figure 8b
557 for a sample of size 200 and various selection coefficients, intermediate- and high-frequency derived
558 variants are more affected by exponential growth and negative selection than the low-frequency
559 derived ones. A plausible reason is that both exponential growth and negative selection enforce an
560 increase of low-frequency derived variants until these classes are saturated and their impact can
561 rather be observed in the complimentary high-frequency allelic classes. In general, this example
562 illustrates nicely that even more elaborated models that include various phases of exponential
563 growth and population declines can be computationally efficiently treated via an appropriate dis-
564 cretization of phases of continuous population size change, using the methods presented in this
565 paper.

566 Acknowledgements

567 We thank the generous support of the Simons Institute for the Theory of Computing, where much
568 of this work was carried out while we were participating in the 2014 program on “Evolutionary
569 Biology and the Theory of Computing.” DZ thanks Anand Bhaskar, Steven N. Evans and Andreas
570 Wollstein for helpful discussions. YSS thanks the Miller Institute for providing a Research Professor-
571 ship while this paper was completed. This research is supported in part by DFG grant STE 325/14
572 from the Priority Program 1590 (DZ, WS), the Volkswagen Foundation grant I/84232 (DZ), an NIH
573 grant R01-GM094402 (MS, YSS), and a Packard Fellowship for Science and Engineering (YSS).

References

574

575 Baake, M., Schlägel, U., 2011. The Peano-Baker series. Proceedings of the Steklov Institute of
576 Mathematics 275, 155–159.

577 Bhaskar, A., Song, Y. S., 2014. Descartes' rule of signs and the identifiability of population demo-
578 graphic models from genomic variation data. Annals of Statistics 42, 2469–2493.

579 Duchen, P., Živković, D., Hutter, S., Stephan, W., Laurent, S., 2013. Demographic inference reveals
580 African and European admixture in the North American *Drosophila melanogaster* population.
581 Genetics 191, 291–301.

582 Evans, S. N., Shvets, Y., Slatkin, M., 2007. Non-equilibrium theory of the allele frequency spectrum.
583 Theoretical Population Biology 71, 109–119.

584 Fisher, R. A., 1930. The Genetical Theory of Natural Selection. Clarendon Press, Oxford.

585 Fu, Y.-X., 1995. Statistical properties of segregating sites. Theoretical Population Biology 48, 172–
586 197.

587 Glinka, S., Ometto, L., Mousset, S., Stephan, W., De Lorenzo, D., 2003. Demography and natu-
588 ral selection have shaped genetic variation in *Drosophila melanogaster*: a multi-locus approach.
589 Genetics 165, 1269–1278.

590 Gravel, S., Henn, B. M., Gutenkunst, R. N., Indap, A. R., Marth, G. T., Clark, A. G., Yu, F., Gibbs,
591 R. A., The 1000 Genomes Project, Bustamante, C. D., 2011. Demographic history and rare allele
592 sharing among human populations. Proceedings of the National Academy of Sciences of the
593 United States of America 108, 11983–11988.

594 Griffiths, R. C., 2003. The frequency spectrum of a mutation, and its age, in a general diffusion
595 model. Theoretical Population Biology 64, 241–251.

596 Griffiths, R. C., Tavaré, S., 1994. Sampling theory for neutral alleles in a varying environment.
597 Philosophical Transactions of the Royal Society B: Biological Sciences 344, 403–410.

598 Griffiths, R. C., Tavaré, S., 1998. The age of a mutation in a general coalescent tree. Stochastic
599 Models 14, 273–295.

- 600 Gutenkunst, R. N., Hernandez, R. D., Williamson, S. H., Bustamante, C. D., 2009. Inferring the joint
601 demographic history of multiple populations from multidimensional SNP frequency data. *PLoS*
602 *Genetics* 5, e1000695.
- 603 Kaj, I., Krone, S. M., 2003. The coalescent process in a population of stochastically varying size.
604 *Journal of Applied Probability* 40, 33–48.
- 605 Karlin, S., Taylor, H., 1981. *A Second Course in Stochastic Processes*. Academic Press.
- 606 Kimura, M., 1955a. Solution of a process of random genetic drift with a continuous model. *Pro-*
607 *ceedings of the National Academy of Sciences of the United States of America* 41, 144–150.
- 608 Kimura, M., 1955b. Random genetic drift in multi-allelic locus. *Evolution* 9, 419–435.
- 609 Kimura, M., 1955c. Stochastic processes and distribution of gene frequencies under natural se-
610 lection. In: *Cold Spring Harbor Symposia on Quantitative Biology*. Vol. 20. Cold Spring Harbor
611 Laboratory Press, pp. 33–53.
- 612 Kimura, M., 1969. The number of heterozygous nucleotide sites maintained in a finite population
613 due to steady flux of mutations. *Genetics* 61, 893–903.
- 614 Krone, S. M., Neuhauser, C., 1997. Ancestral processes with selection. *Theoretical Population Biol-*
615 *ogy* 51, 210–237.
- 616 Lenski, R. E., 2011. Evolution in action: a 50,000-generation salute to Charles Darwin. *Microbe* 6,
617 30–33.
- 618 Lukić, S., Hey, J., 2012. Demographic inference using spectral methods on SNP data, with an
619 analysis of the human out-of-Africa expansion. *Genetics* 192, 619–639.
- 620 Nei, M., Maruyama, T., Chakraborty, R., 1975. The bottleneck effect and genetic variability in pop-
621 ulations. *Evolution* 29, 1–10.
- 622 Sawyer, S. A., Hartl, D. L., 1992. Population genetics of polymorphism and divergence. *Genetics*
623 132, 1161–1176.
- 624 Slatkin, M., Hudson, R. R., 1991. Pairwise comparisons of mitochondrial DNA sequences in stable
625 and exponentially growing populations. *Genetics* 129, 555–562.

- 626 Song, Y. S., Steinrücken, M., 2012. A simple method for finding explicit analytic transition densities
627 of diffusion processes with general diploid selection. *Genetics* 190, 1117–1129.
- 628 Steinrücken, M., Bhaskar, A., Song, Y. S., 2014. A novel spectral method for inferring general
629 diploid selection from time series genetic data. *Annals of Applied Statistics* 8, 2203–2222.
- 630 Steinrücken, M., Wang, Y., Song, Y. S., 2013. An explicit transition density expansion for a multi-
631 allelic Wright–Fisher diffusion with general diploid selection. *Theoretical Population Biology* 83,
632 1–14.
- 633 Stephan, W., Li, H., 2007. The recent demographic and adaptive history of *Drosophila melanogaster*.
634 *Heredity* 98, 65–68.
- 635 Tennessen, J. A., Bigham, A. W., O’Connor, T. D., Fu, W., Eimear, E., *et al.*, 2012. Evolution and
636 functional impact of rare coding variation from deep sequencing of human exomes. *Science* 337,
637 64–69.
- 638 Watterson, G. A., 1984. Allele frequencies after a bottleneck. *Theoretical Population Biology* 26,
639 387–407.
- 640 Williamson, S. H., Hernandez, R., Fledel-Alon, A., Zhu, L., Nielsen, R., Bustamante, C. D., 2005.
641 Simultaneous inference of selection and population growth from patterns of variation in the
642 human genome. *Proceedings of the National Academy of Sciences of the United States of America*
643 102, 7882–7887.
- 644 Wooding, S., Rogers, A., 2002. The matrix coalescent and an application to human single-nucleotide
645 polymorphisms. *Genetics* 161, 1641–1650.
- 646 Zhao, L., Yue, X., Waxman, D., 2013. Complete numerical solution of the diffusion equation of
647 random genetic drift. *Genetics* 194, 973–985.
- 648 Živković, D., Stephan, W., 2011. Analytical results on the neutral non-equilibrium allele frequency
649 spectrum based on diffusion theory. *Theoretical Population Biology* 79, 184–191.
- 650 Živković, D., Wiehe, T., 2008. Second-order moments of segregating sites under variable population
651 size. *Genetics* 180, 341–357.

652

Appendix. Derivation of (12)

653 Here, we derive the expression shown in (12). Using (2), (5), and (7), note that

$$\begin{aligned} \int_0^1 \pi_i(z) \Phi_n^i(z) \Phi_m^{i+1}(z) dz &= \int_0^1 \frac{c_i e^{2c_i \sigma z}}{z(1-z)} \sum_{k=0}^{\infty} u_{n,k}^i H_k^i(z) \sum_{l=0}^{\infty} u_{m,l}^{i+1} H_l^{i+1}(z) dz \\ &= \sqrt{\frac{c_i}{c_{i+1}}} \sum_{k=0}^{\infty} \sum_{l=0}^{\infty} u_{n,k}^i u_{m,l}^{i+1} \int_0^1 \frac{e^{\sigma z(c_i - c_{i+1})}}{z(1-z)} G_k(z) G_l(z) dz. \end{aligned} \quad (\text{A.1})$$

654 Without loss of generality, assume $c_i \neq c_{i+1}$. (If $c_i = c_{i+1}$, the integral in (A.1) is trivial to evaluate
655 using orthogonality.) Since $z^{-1}(1-z)^{-1}G_k(z)G_l(z)$ is a polynomial of order $k+l+2$, its j th
656 derivative vanishes for $j \geq k+l+3$. Using integration by parts recursively $k+l+2$ times, we
657 obtain

$$\int_0^1 \frac{e^{\sigma z(c_i - c_{i+1})}}{z(1-z)} G_k(z) G_l(z) dz = \sum_{j=0}^{k+l+2} (-1)^j \left[\frac{e^{\sigma z(c_i - c_{i+1})}}{[\sigma(c_i - c_{i+1})]^{j+1}} \frac{\partial^j}{\partial z^j} \left\{ \frac{G_k(z) G_l(z)}{z(1-z)} \right\} \right]_0^1.$$

658 Note that the summand for $j=0$ in the previous equation is equal to zero and will be omitted in
659 the remainder. Since $G_k(1-z) = (-1)^k G_k(z)$, we have

$$\left. \frac{\partial^j}{\partial z^j} \left\{ \frac{G_k(z) G_l(z)}{z(1-z)} \right\} \right|_{z=0} = (-1)^{k+l+j} \left. \frac{\partial^j}{\partial z^j} \left\{ \frac{G_k(z) G_l(z)}{z(1-z)} \right\} \right|_{z=1},$$

660 so that

$$\int_0^1 e^{\sigma z(c_i - c_{i+1})} \frac{G_k(z) G_l(z)}{z(1-z)} dz = \sum_{j=1}^{k+l+2} (-1)^j \frac{e^{\sigma(c_i - c_{i+1})} - (-1)^{k+l+j}}{\{\sigma(c_i - c_{i+1})\}^{j+1}} \left. \frac{\partial^j}{\partial z^j} \left\{ \frac{G_k(z) G_l(z)}{z(1-z)} \right\} \right|_{z=1}. \quad (\text{A.2})$$

661 The modified Gegenbauer polynomials are defined as

$$G_n(x) = -x(1-x)(n+1) \cdot {}_2F_1(-n, n+3; 2; 1-x),$$

662 where ${}_2F_1(a, b; c; z) = \sum_{j \geq 0} a_{(j)} b_{(j)} / c_{(j)} z^j / j!$ is the Gauss hypergeometric function,
663 $d_{(0)} = 1$, and $d_{(j)} = d(d+1) \cdots (d+j-1)$, $j \geq 1$. Applying this definition, we obtain

$$\frac{\partial^j}{\partial z^j} \left\{ \frac{G_k(z)G_l(z)}{z(1-z)} \right\} \Big|_{z=1} = (k+1)(l+1) \sum_{u=0}^k \sum_{v=0}^l \frac{(-k)_{(u)}(k+3)_{(u)}}{2_{(u)}u!} \frac{(-l)_{(v)}(l+3)_{(v)}}{2_{(v)}v!} \times \frac{\partial^j}{\partial z^j} \{z(1-z)^{u+v+1}\} \Big|_{z=1}.$$

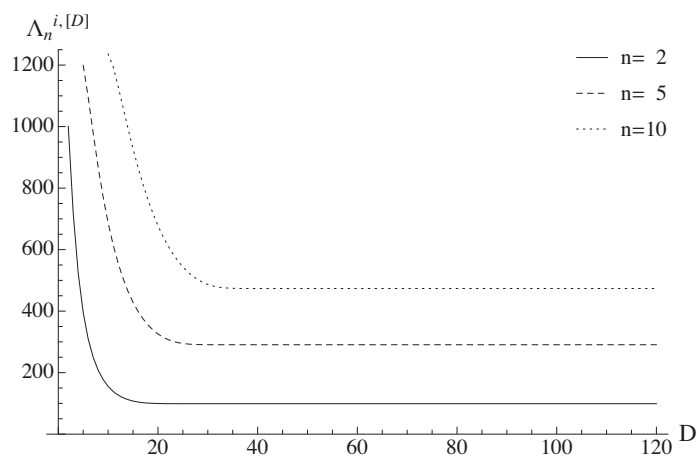
664 Note that the sums are finite, since $(-a)_{(b)} = 0$ for integers $a < b$. It is simple to show that

$$\frac{\partial^j}{\partial z^j} \{z(1-z)^{u+v+1}\} \Big|_{z=1} = \begin{cases} (-1)^j j!, & j = u + v + 1, \\ (-1)^{j-1} j!, & j = u + v + 2, \\ 0, & \text{otherwise.} \end{cases}$$

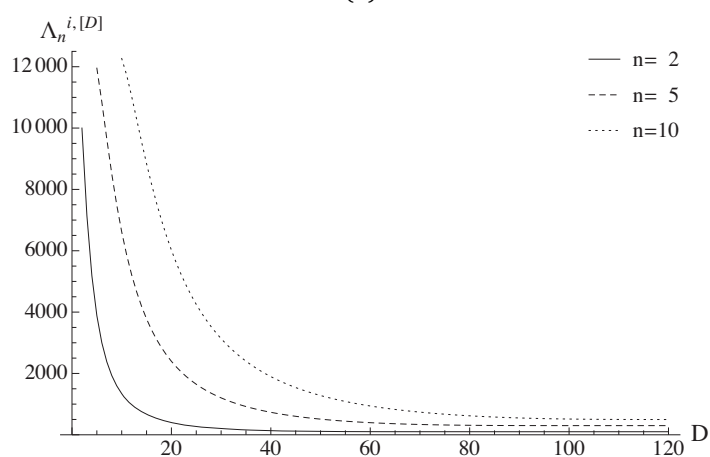
665 By applying this result we obtain, after some algebra,

$$\begin{aligned} \frac{\partial^j}{\partial z^j} \left\{ \frac{G_k(z)G_l(z)}{z(1-z)} \right\} \Big|_{z=1} &= (k+1)(k+1)(k+2)(l+1) \\ &\quad \times (-1)^{j+1} \sum_{r=0}^{j-1} \binom{j}{r} \frac{(-k)_{(j-r-2)}(k+3)_{(j-r-2)}}{2_{(j-r-2)}} \frac{(-l)_{(r)}(l+3)_{(r)}}{2_{(r)}} \\ &= -\frac{k+1}{l+2} \sum_{r=0}^{j-1} \frac{j!(l+r+2)!(k+j-r)!}{r!(r+1)!(j-r)!(j-r-1)!(l-r)!(k-(j-r-2))!} \\ &= -\frac{(k+1)(l+1)j!}{(k+2)(l+2)} \sum_{r=0}^{j-1} \binom{k+2}{j-r} \binom{k+j-r}{j-r-1} \binom{l+r+2}{r+1} \binom{l}{r}. \quad (\text{A.3}) \end{aligned}$$

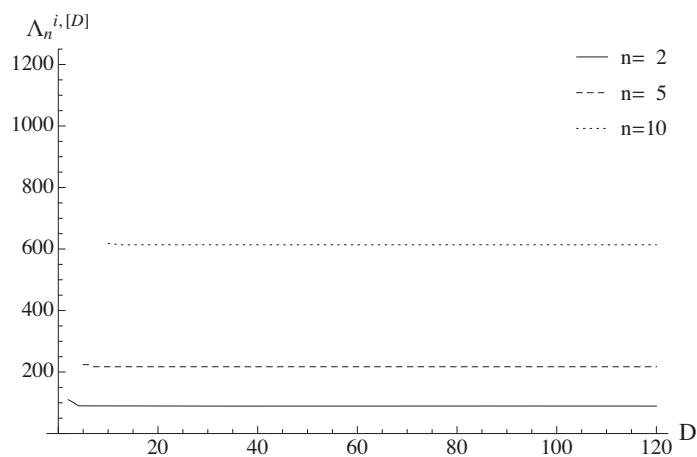
666 Finally, combining (A.3), (A.2), and (A.1) yields the desired result.



(a)



(b)



(c)

Figure 1 Convergence of the eigenvalues $\Lambda_n^{i,[D]}$ with increasing truncation level D for (a) a constant population size ($c_i = 1$), (b) a large population ($c_i = 10$) and (c) a small population ($c_i = 1/10$). The eigenvalues are plotted for three values of n and a scaled selection coefficient of $\sigma = 100$ in each panel.

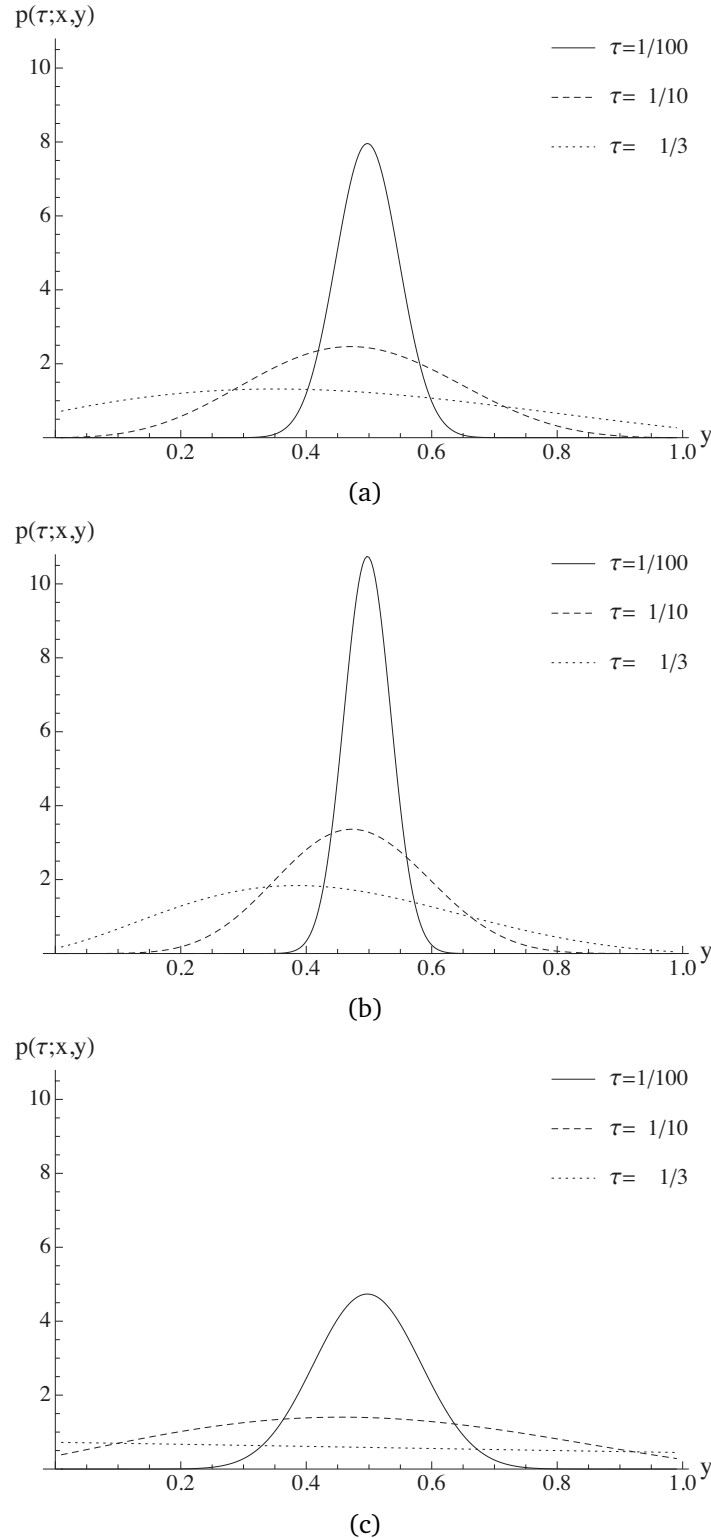


Figure 2 Transition densities for various transition times τ and a fixed selection coefficient $\sigma = -1$. In all cases, we set $x = 1/2$ and $D = 100$. (a) A single-epoch model ($K = 1$), a constant population size with $c_0 = 1$ (b) A two-epoch model ($K = 2$), with an instantaneous expansion ($c_0 = 1, c_1 = 10, t_1 = \tau/2$). (c) A three-epoch model ($K = 3$), with a population bottleneck followed by an expansion ($c_0 = 1, c_1 = 1/10, c_2 = 10, t_1 = \tau/4, t_2 = \tau/2$).

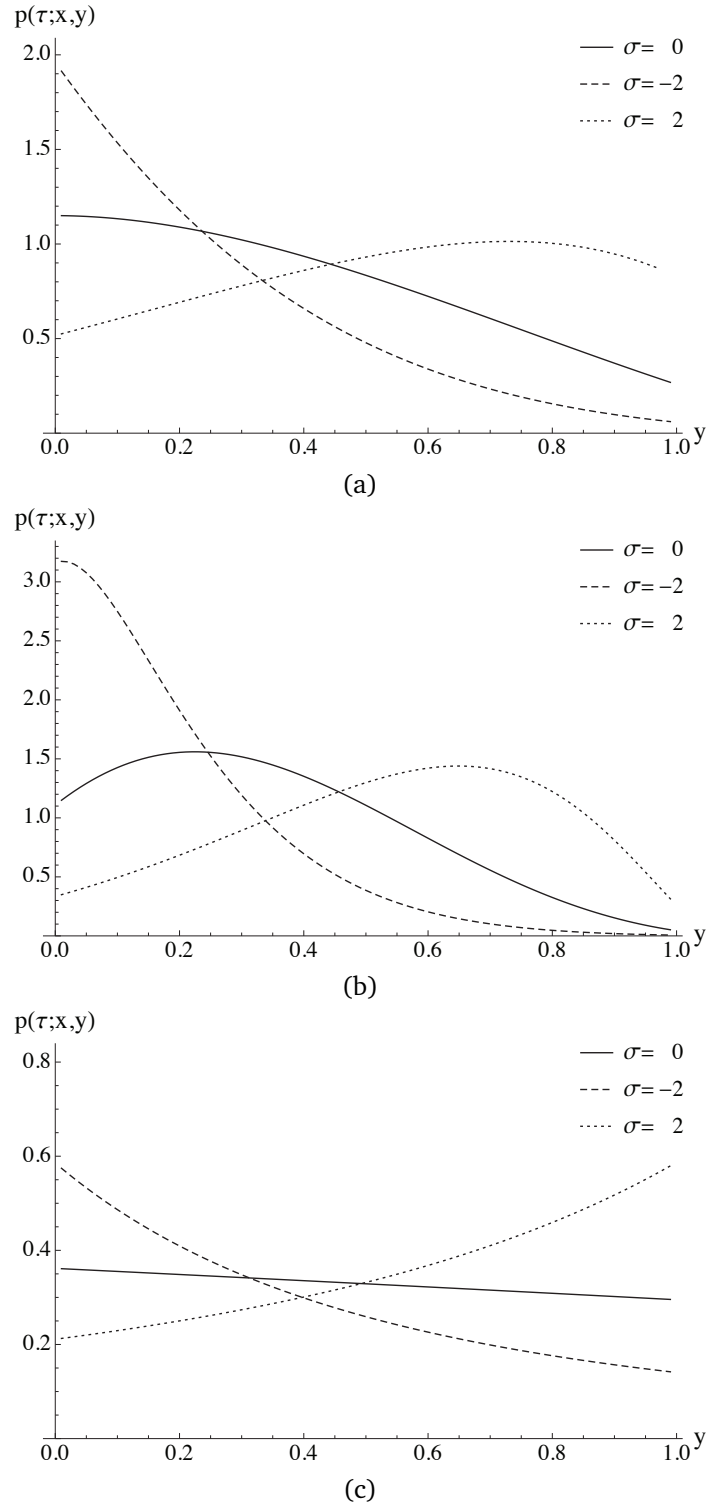


Figure 3 Transition densities for various selection coefficients σ and a fixed transition time $\tau = 1/2$. In all cases, we set $x = 1/3$ and $D = 100$. (a) A single-epoch model ($K = 1$), a constant population size with $c_0 = 1$. (b) A two-epoch model ($K = 2$), with an instantaneous expansion ($c_0 = 1, c_1 = 10, t_1 = \tau/2$). (c) A three-epoch model ($K = 3$), with a population bottleneck followed by an expansion ($c_0 = 1, c_1 = 1/10, c_2 = 10, t_1 = \tau/4, t_2 = \tau/2$).

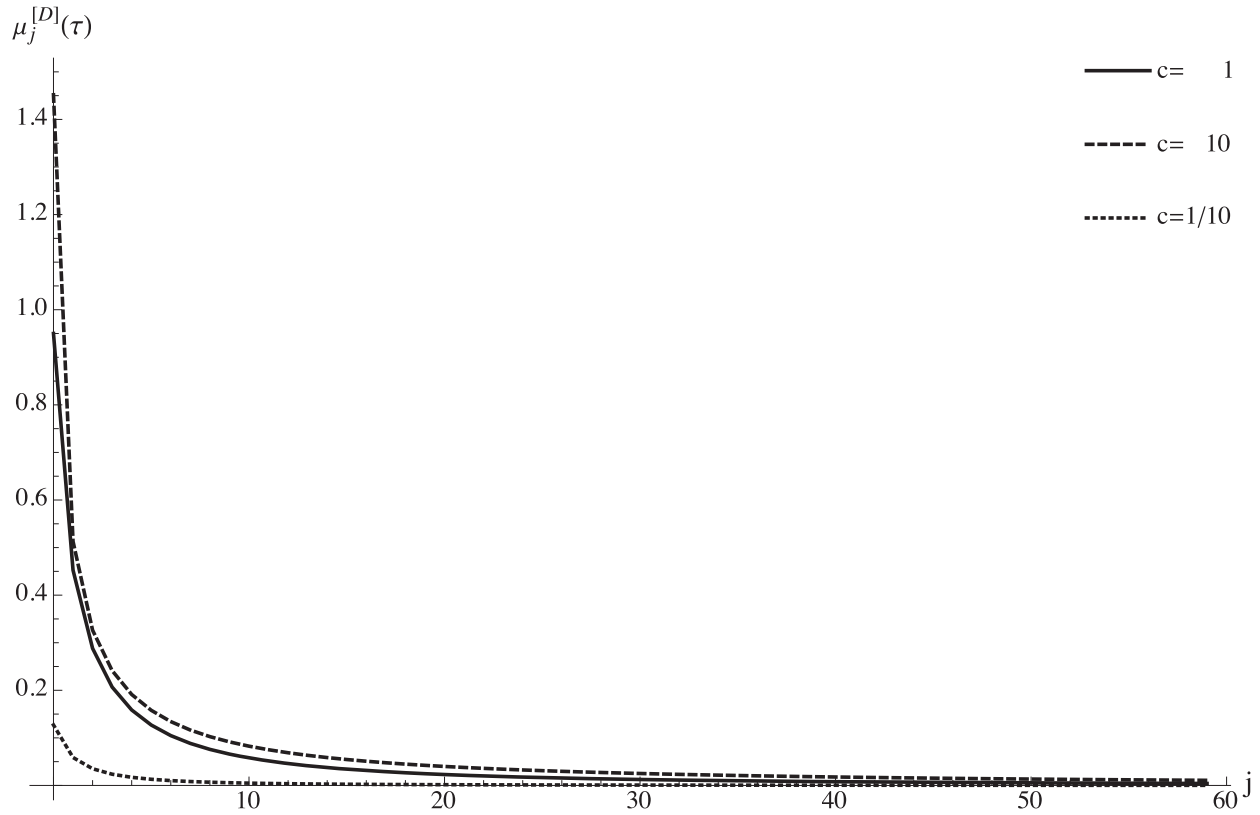


Figure 4 Convergence of the moments $\mu_j^{[D]}(\tau)$ as j increases, with $D = 500$, $\tau = 1/4$ and $\sigma = 10$. The moments are in equilibrium until time zero, when the population size is either kept constant to $c = 1$ or instantaneously changed to $c = 10$ or $c = 1/10$.

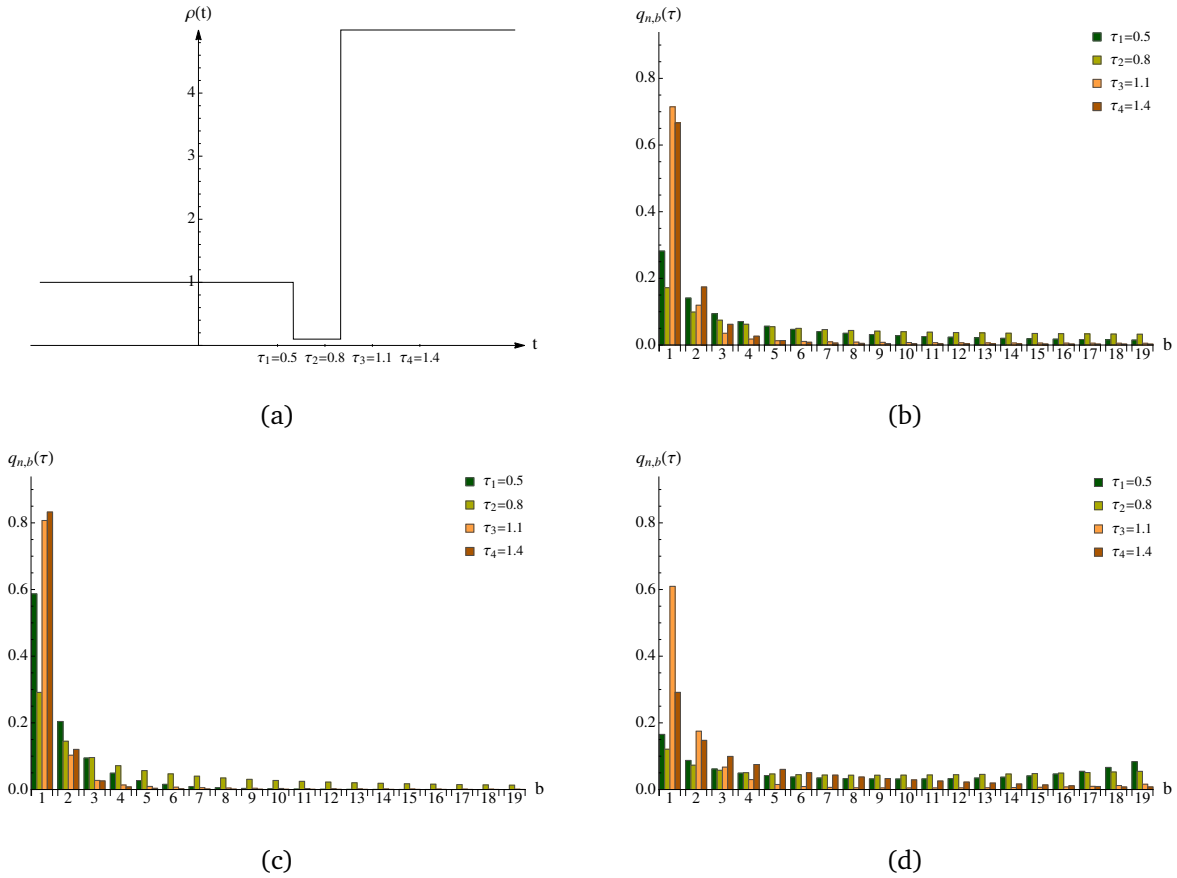


Figure 5 (a) The relative population size, $\rho(t)$, is initially 1 and changes instantaneously to 1/10 and 5 at times 6/10 and 9/10, respectively. The SFS of a sample of size 20 are plotted for this demography (b) without selection, (c) negative selection of $\sigma = -2$ and (d) positive selection of $\sigma = 10$. The times of sampling are illustrated in (a) and the bars are accordingly displayed from the left to the right.

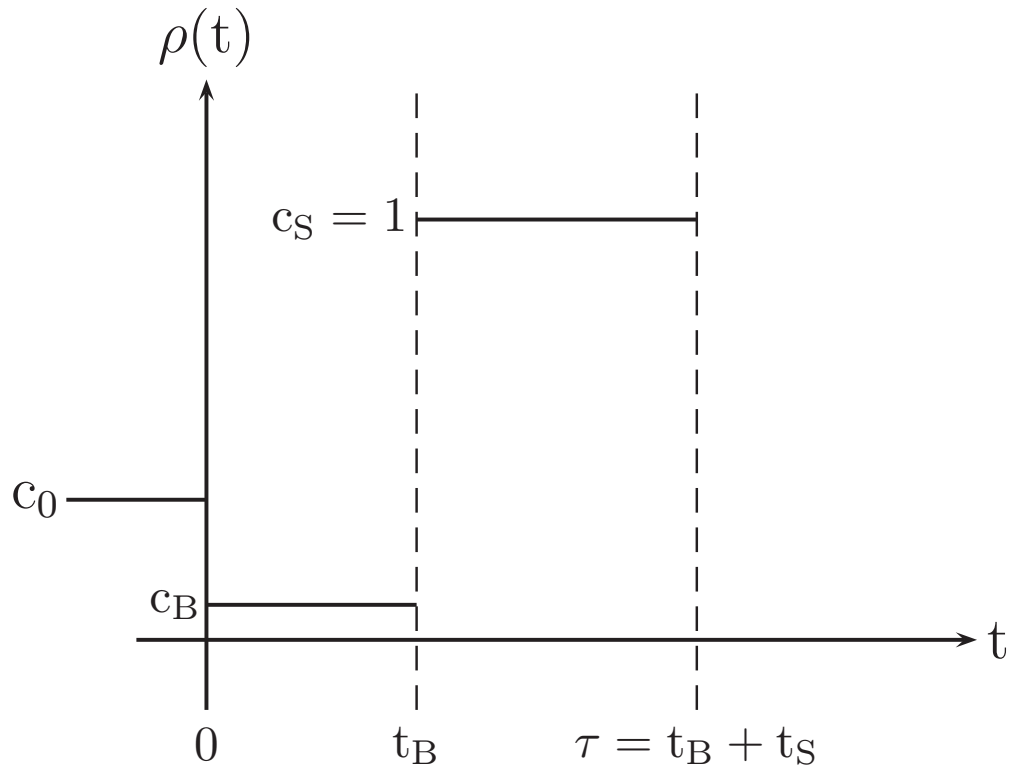


Figure 6 The population is constant in size before being instantaneously changed to relative size c_B at time zero. Then, another jump to relative population size c_S follows at time t_B , before a sample is taken at time $\tau = t_B + t_S$.

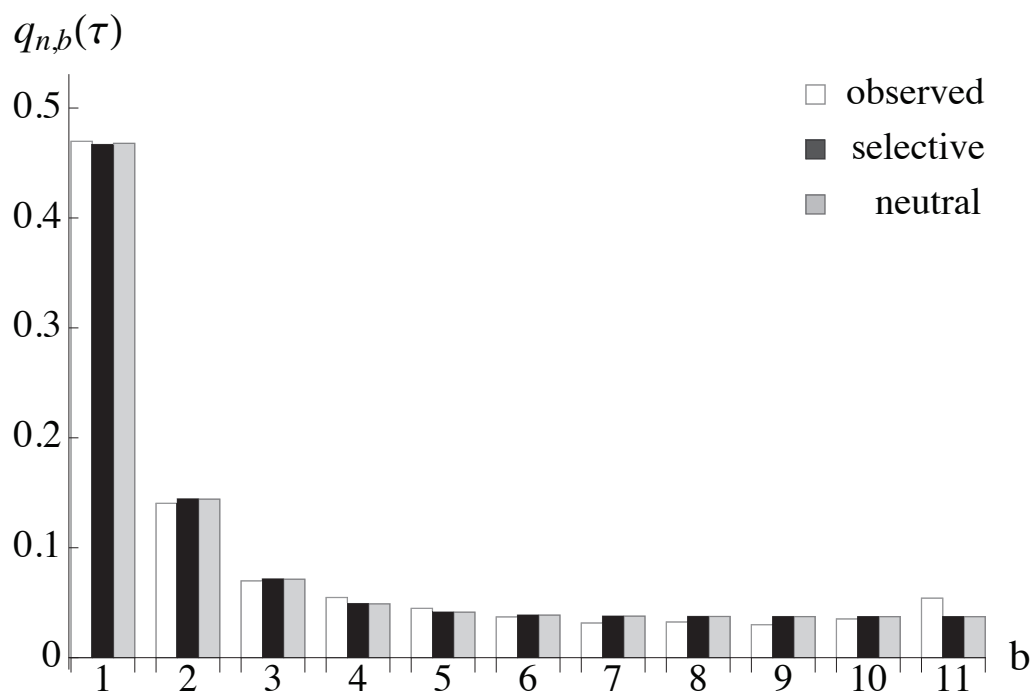


Figure 7 (a) SFS for the observed data and the most likely selective and neutral parameter estimates from left to right.

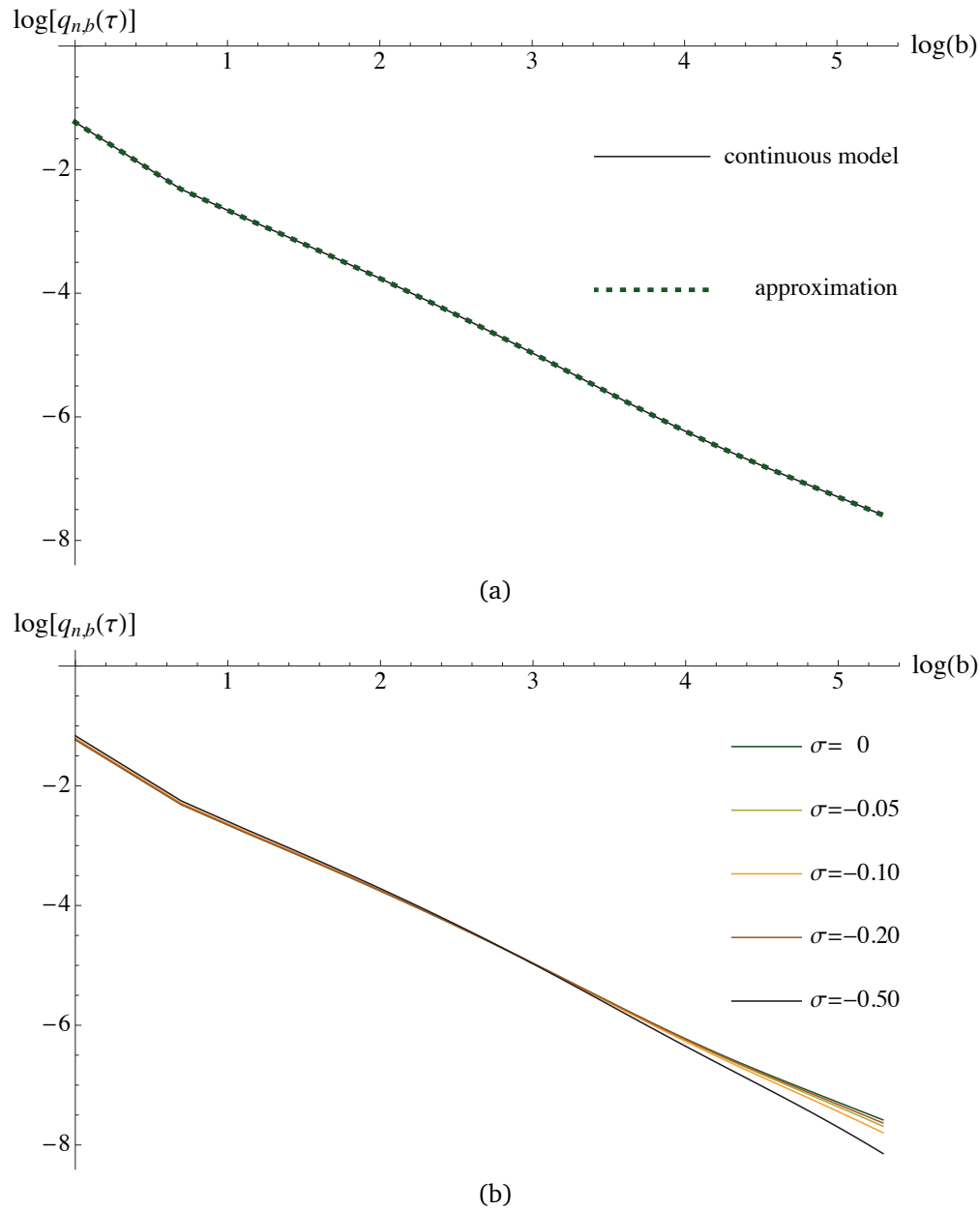


Figure 8 (a) Log-log plots for the SFS of the continuous and the discretized version of the estimated human African demography and neutral evolution. (b) Log-log plots for the SFS of the discretized version under various selection coefficients. The selection coefficients in the legend are ordered from top to bottom according to the function values of the high-frequency derived alleles. The sample size is given by $n = 200$ in both subfigures.

Table 1 Grid values chosen for each parameter in our optimization procedure

c_0	0.011	0.023	0.05	0.1	0.224	0.5	1	2.154	4.642	10	
σ	-10	-5.848	-3.420	-2	-1.260	-0.79	-0.5	-0.292	-0.171	-0.1	0
c_B	0.001	0.0022	0.005	0.011	0.023	0.05	0.1	0.224	0.5	1	
t_B	0.001	0.0022	0.005	0.011	0.023	0.05	0.1	0.224	0.5	1	
t_S	0.001	0.0022	0.005	0.011	0.023	0.05	0.1	0.224	0.5	1	

The underlying bottleneck model is illustrated in Figure 6. Grid values $c_0 \geq c_B$ are considered for the 5-parameter model, whereas $c_0 = c_S$ in the 4-parameter model. The grid values for the remaining parameters are applied in both scenarios. The ratio of two consecutive values remains constant between (and including the) two subsequent bold entries.

Table 2 Parameter estimation results based on 10,000 sampled sites

		\hat{c}_0	$\hat{\sigma}$	\hat{c}_B	\hat{t}_B	\hat{t}_S
True parameters		0.5	0 or -2	0.1	0.1	0.05
(A1)	5%	0.5		0.1	0.1	0.05
	Median	0.5		0.1	0.1	0.05
	95%	0.5		0.1	0.1	0.05
(A2)	5%	0.22		0.02	0.005	0.05
	Median	0.22		0.1	0.05	0.05
	95%	0.22		0.1	0.05	0.05
(A3)	5%	0.22	-2	0.05	0.01	0.05
	Median	0.5	-2	0.1	0.1	0.05
	95%	0.5	0	0.1	0.1	0.05
(A4)	5%	0.5	-0.5	0.1	0.001	0.05
	Median	0.5	0	0.1	0.1	0.05
	95%	2.15	0	0.1	0.1	0.05

SFS were computed for the true parameters and the demography illustrated in Figure 6 ($c_0 = 1/2$, $c_S = 1$). Then, 10,000 sites were sampled according to the SFS of the neutral and the selective scenario, and this procedure was repeated 200 times each. The log-likelihood values were maximized over the parameter spaces as specified in the main text, and the table reports the median, the 0.05 and the 0.95 quantiles. The four cases correspond to assuming (A1) neutrality when $\sigma = 0$, (A2) neutrality when $\sigma = -2$, (A3) presence of selection when $\sigma = -2$, and (A4) presence of selection when $\sigma = 0$.

Table 3 Parameter estimation results based on the expected SFS assuming neutrality when the true model is under selection

Selection coefficient	$\sigma = -1/2$	$\sigma = -2$
Demographic model	$(\hat{c}_0, \hat{c}_B, \hat{t}_B, \hat{t}_S)$	$(\hat{c}_0, \hat{c}_B, \hat{t}_B, \hat{t}_S)$
Constant population size	$(0.500, 1.00, 1.10 - \hat{t}_S, \hat{t}_S)$	$(0.100, 1.000, 0.523 - \hat{t}_S, \hat{t}_S)$
Bottleneck with $t_S = 1/200$	$(0.224, 0.05, 0.05, 0.002)$	$(0.224, 0.100, 0.050, 0.005)$
Bottleneck with $t_S = 1/20$	$(0.500, 0.10, 0.10, 0.050)$	$(0.224, 0.100, 0.050, 0.050)$
Bottleneck with $t_S = 1/2$	$(1.000, 0.05, 0.10, 0.500)$	$(0.100, 1.000, 0.324 - \hat{t}_S, \hat{t}_S)$

SFS were computed for the following demographic scenarios and selection coefficients. In terms of the demography, either a constant population size was assumed, or a bottleneck model according to Figure 6 with parameters $c_0 = 1/2$, $c_B = 1/10$, $c_S = 1$, $t_B = 1/10$ and $t_S = 1/200$, $1/20$ or $1/2$. The selection coefficients are $\sigma = -1/2$ and -2 . The parameter estimates were obtained according to the procedure and the parameter spaces described in the main text and by assuming neutrality in each case. In the first row, and in the forth row, second column, we obtained $\hat{c}_B = 1$, i.e. an instantaneous expansion occurs as the only size change $\hat{t}_B + \hat{t}_S$ before sampling.

Table 4 Parameter estimation results based on 10,000 sampled sites when the ancestral population size c_0 is incorrectly assumed to equal the current size c_S , while the true model has $c_0 = 1/2$ and $c_S = 1$.

		c_0	$\hat{\sigma}$	\hat{c}_B	\hat{t}_B	\hat{t}_S
True parameters		0.5	0 or -2	0.1	0.1	0.05
(A1)	5%			0.1	0.22	0.02
	Median			0.1	0.22	0.05
	95%			0.22	0.5	0.05
(A2)	5%			0.1	0.22	0.05
	Median			0.1	0.22	0.05
	95%			0.22	1	0.05
(A3)	5%		-0.79	0.1	0.22	0.05
	Median		-0.79	0.1	0.22	0.05
	95%		-0.5	0.1	0.22	0.05
(A4)	5%		-1.26	0.01	0.01	0.05
	Median		-1.26	0.05	0.05	0.05
	95%		-0.79	0.1	0.1	0.1

SFS were computed for the true parameters and the demography illustrated in Figure 6 ($c_0 = 1/2$, $c_S = 1$). Then, 10,000 sites were sampled according to the SFS of the neutral and the selective scenario, and this procedure was repeated 200 times each. The log-likelihood values were maximized over the 4-parameter space (where $c_0 = c_S$ is assumed), and the table reports the median, the 0.05 and the 0.95 quantiles. The four cases correspond to assuming (A1) neutrality when $\sigma = 0$, (A2) neutrality when $\sigma = -2$, (A3) presence of selection when $\sigma = -2$, and (A4) presence of selection when $\sigma = 0$.

Table 5 Parameter estimation results based on the expected SFS when the ancestral population size c_0 is incorrectly assumed to equal the current size c_S , while the true model has $c_0 = 1/2$ and $c_S = 1$.

Selection coefficient	$\sigma = 0$	$\sigma = -1/2$	$\sigma = -2$
Demographic model	$(\hat{\sigma}, \hat{c}_B, \hat{t}_B, \hat{t}_S)$ $(\hat{c}_B, \hat{t}_B, \hat{t}_S)$	$(\hat{\sigma}, \hat{c}_B, \hat{t}_B, \hat{t}_S)$ $(\hat{c}_B, \hat{t}_B, \hat{t}_S)$	$(\hat{\sigma}, \hat{c}_B, \hat{t}_B, \hat{t}_S)$ $(\hat{c}_B, \hat{t}_B, \hat{t}_S)$
Bottleneck with $t_S = 1/200$	$(-3.420, 0.023, 0.050, 0.001)$ $(0.224, 0.224, 0.011)$	$(-0.171, 0.224, 0.224, 0.011)$ $(0.224, 0.224, 0.011)$	$(-5.848, 0.023, 0.050, 0.001)$ $(0.023, 0.100, 0.001)$
Bottleneck with $t_S = 1/20$	$(-1.260, 0.050, 0.050, 0.050)$ $(0.100, 0.224, 0.050)$	$(-2., 0.050, 0.050, 0.050)$ $(0.100, 0.224, 0.050)$	$(-0.794, 0.100, 0.224, 0.050)$ $(0.100, 0.224, 0.050)$
Bottleneck with $t_S = 1/2$	$(-0.292, 0.224, 0.500, 0.500)$ $(0.224, 0.500, 0.500)$	$(0, 0.050, 0.100, 0.500)$ $(0.050, 0.100, 0.500)$	$(-2., 0.224, 0.500, 0.500)$ $(0.050, 0.224, 0.500)$

SFS were computed for the following demographic scenarios and selection coefficients. In terms of the demography, a bottleneck model was assumed according to Figure 6 with parameters $c_0 = 1/2$, $c_B = 1/10$, $t_B = 1/10$ and $t_S = 1/200$ or $1/2$. The selection coefficients were chosen as $\sigma = 0$, $-1/2$ and -2 . The parameter estimates were obtained according to the model assuming $c_0 = c_S$ (the grid for the 4-parameter space being a subset of the grid for the 5-parameter space) and by assuming either selection or neutrality in each case.

Table 6 Parametric bootstrap results for the *Drosophila melanogaster* data

	$\hat{\sigma}$	c_0	\hat{c}_B	\hat{t}_B	\hat{t}_S
MLE	0	1	0.05	0.1	0.1
5%	-0.794	0.5 0.5	0.002 0.023	0.002 0.023	0.1 0.1
Median	-0.171	1 1	0.050 0.050	0.100 0.100	0.1 0.1
95%	0	10 10	0.050 0.100	0.224 0.224	0.1 0.1

The demographic history was estimated with and without selection for the demographic model illustrated in Figure 6 for the entire dataset of 3234 polymorphic sites. The estimation procedure is described in the main text. The estimated parameters given at the top of the table were used to generate 200 frequency spectra consisting of 3234 polymorphic sites each for the neutral and the selective model, respectively. We estimated the neutral demography for each neutral subsample and the demography with selection for each selective dataset, before the median, the 0.05 and the 0.95 quantiles were evaluated.

Table 7 Estimated parameters and their likelihoods for the *Drosophila melanogaster* data for fixed values of c_0

c_0	$\hat{\sigma}$	\hat{c}_B	\hat{t}_B	\hat{t}_S	L
1.00	0	0.001	0.0015	0.1566	-5963.888
1.67	0	0.001	0.0020	0.1614	-5963.208
2.45	0	0.001	0.0024	0.1647	-5963.027
3.59	0	0.001	0.0028	0.1614	-5962.965
4.08	0	0.001	0.0029	0.1638	-5962.924
5.99	-0.007	0.001	0.0032	0.1655	-5962.913
6.81	-0.005	0.001	0.0034	0.1655	-5962.902
7.74	-0.002	0.001	0.0035	0.1655	-5962.890
8.80	0	0.001	0.0037	0.1638	-5962.884
10.0	-0.007	0.001	0.0038	0.1647	-5962.894

The demographic history was analyzed with and without selection for the demographic model illustrated in Figure 6 for the entire dataset of 3234 polymorphic sites. The maximum likelihood estimates and their likelihood values L were obtained for various predefined ancestral population sizes and based on a gradually refined grid as described in the main text.

Table 8 Parameter ranges of the most likely estimates for the *Drosophila melanogaster* data for fixed values of c_0

c_0	$\hat{\sigma}$	\hat{c}_B	\hat{t}_B/\hat{c}_B	\hat{t}_S	L
1.00	[-0.010, 0]	[0.001, 0.0026]	[1.49, 1.49]	[0.1541, 0.1591]	[-5963.926, -5963.888]
1.67	[-0.007, 0]	[0.001, 0.0021]	[2.00, 2.00]	[0.1598, 0.1630]	[-5963.233, -5963.208]
2.45	[-0.010, 0]	[0.001, 0.0018]	[2.37, 2.37]	[0.1622, 0.1663]	[-5963.050, -5963.027]
3.59	[-0.015, 0]	[0.001, 0.0026]	[2.74, 2.77]	[0.1598, 0.1680]	[-5962.981, -5962.965]
4.08	[-0.007, 0]	[0.001, 0.0021]	[2.89, 2.89]	[0.1622, 0.1663]	[-5962.949, -5962.924]
5.99	[-0.015, 0]	[0.001, 0.0021]	[3.25, 3.25]	[0.1622, 0.1688]	[-5962.939, -5962.913]
6.81	[-0.010, 0]	[0.001, 0.0021]	[3.38, 3.38]	[0.1622, 0.1688]	[-5962.926, -5962.902]
7.74	[-0.007, 0]	[0.001, 0.0018]	[3.52, 3.52]	[0.1622, 0.1680]	[-5962.912, -5962.890]
8.80	[-0.003, 0]	[0.001, 0.0026]	[3.66, 3.66]	[0.1614, 0.1655]	[-5962.914, -5962.884]
10.0	[-0.022, 0]	[0.001, 0.0026]	[3.71, 3.75]	[0.1614, 0.1688]	[-5962.927, -5962.894]

The demographic history was analyzed with and without selection for the demographic model illustrated in Figure 6 for the entire dataset of 3234 polymorphic sites. The set of the 100 likeliest parameter combinations was respectively estimated for various predefined ancestral population sizes and based on a gradually refined grid as described in the main text. From this set, the two outermost estimates were chosen for each single parameter and for the likelihood value L to obtain the outlined parameter ranges.